



TALLINN UNIVERSITY OF TECHNOLOGY
SCHOOL OF SCIENCE
DEPARTMENT OF CYBERNETICS

**ENHANCING THE SENSITIVITY OF NUCLEAR MAGNETIC RESONANCE
SPECTROSCOPY WITH PARAHYDROGEN HYPERPOLARISATION AND TO
APPLY IT IN CANCER DIAGNOSTICS**

Master's thesis

Student: Helen Pais

Student code: 212095YAFM

Supervisors: Indrek Reile

Kerti Ausmees

National Institute of Chemical Physics and Biophysics

Study program: Applied Physics

Tallinn 2023

Declaration

Hereby I declare that I have compiled the paper independently and all works, important standpoints and data by other authors have been properly referenced and the same paper has not been previously been presented for grading.

Author: Helen Pais
(signature)

Date:

The paper conforms to requirements in force.

Supervisors: Indrek Reile, Kerti Ausmees
(signature)

Date:

Permitted to the defence.

Chairman of
the Defence
Committee:

.....
(signature)

Kuupäev:

Table of contents

Introduction	7
1 NMR spectroscopy	8
1.1 Physical background	8
1.1.1 Atoms and their parameters in NMR	8
1.1.2 Chemical shift	11
1.1.3 Fourier transformation	12
1.1.4 Relaxation	14
1.1.4.1 Longitudinal magnetisation and relaxation	15
1.1.4.2 Transverse magnetisation and relaxation	18
1.2 Hyperpolarisation	21
2 Blood and diagnostics	24
3 Energy metabolism of cancerous cells	25
4 Aims of the present work	27
5 Method development	28
5.1 Technical details	28
5.1.1 NMR spectrometers and used equipment	28
5.1.2 Reagents and stock solutions	29
5.1.3 Sample preparation for NMR experiments	30
5.2 Results and discussion	33
5.2.1 Relaxation dependance on temperature and magnetic field	35
5.2.1.1 Optimal temperature for hyperpolarisation experiments	35
5.2.1.2 Temperature influence on T_1 and T_2 relaxation on 800 MHz spectrometer	38
5.2.1.3 T_1 and T_2 relaxation in different magnetic fields	46
5.2.1.4 Summary	52
5.2.2 ATP, ADP, AMP and blood NMR	53
5.2.2.1 ATP, ADP and AMP with Mg^{2+} detection	54
5.2.2.2 ATP nh-PHIP signal enhancement by 2H -labelled iridium complex	58
5.2.2.3 Two-valence-electron metal ions removal process	59
5.2.2.4 EDTA	62
5.2.2.5 Summary	67
5.3 Summary of experimental results	67

Summary	69
Acknowledgements	71
Bibliography	72
Appendices	75
Appendix 1. Tables with T_1 and T_2 relaxation time constants	75

Abstract

In this work, the relaxation of nh-PHIP catalyst complexes has been studied using nuclear magnetic resonance spectroscopy. The relaxation time constants T_1 and T_2 in nh-PHIP are influenced by temperature, magnetic field strength and ^2H labelling of the nh-PHIP catalyst complex.

In addition, human whole blood and biologically relevant analytes were studied in order to later apply the optimised conditions found in the relaxation experiments to the nh-PHIP analysis of human blood for the detection of ATP, ADP and AMP. However, adenosine phosphates are complexed with Mg^{2+} in human blood, which is the reason why they are undetectable with nh-PHIP. Further studies are needed to find a way to remove the complexation of adenosine phosphates with magnesium in order to annotate them from the whole blood.

Abbreviations and terms

Ade	abbreviation for adenosine in chemical complexes
ADP	adenosine diphosphate
AMP	adenosine monophosphate
ATP	adenosine triphosphate
FID	free induction decay (NMR signal, exponentially decaying oscillation)
ppm	parts per million
IMes	abbreviation of chemical $[\text{Ir}(\text{Cl})(\text{COD})(\text{IMes})]$
Mg-ADP	adenosine diphosphate magnesium salt
Mg-AMP	adenosine monophosphate magnesium salt
Mg-ATP	adenosine triphosphate magnesium salt
mtz	1-methyl-1,2,3-triazole
NA	abbreviation for nicotinamide in chemical complexes
nh-PHIP	non-hydrogenative <i>parahydrogen</i> induced polarization
NMR	nuclear magnetic resonance
RBC	red blood cell
TMS	tetramethylsilane ($\text{Si}(\text{CH}_3)_4$)
WBC	white blood cell
X	denotes adenosine or nicotinamide in chemical complexes (e.g., $[\text{Ir}(\text{H})_2(\text{IMes})(\text{mtz})_2\text{X}]^+$)
Y	denotes ATP, adenosine or nicotinamide in chemical complexes (e.g., $[\text{Ir}(\text{H})_2(\text{IMes})(\text{mtz})_2\text{Y}]^+$)
ZQ-COSY	zero-quantum correlated spectroscopy

Introduction

Cancer is a subject of significant public interest along with its early detection and treatment. Major modifications between normal and cancer cells appear in energy metabolism. Energy production process results in adenosine triphosphate (ATP). Adenosine diphosphate and adenosine monophosphate are closely associated with ATP. Their levels and ratios may represent change in normal versus cancer cells energy metabolism. And with that excess ATP might be present in blood. It is desired to detect ATP from the blood plasma for early detection of cancer.

Nuclear magnetic resonance (NMR) spectroscopy is a powerful analytical tool. However, it has low sensitivity. ATP concentration in plasma is below detection limit of regular NMR, which is the reason why it cannot be studied. Recent progress in NMR methodology has allowed to improve the sensitivity of NMR in biofluids using hyperpolarisation. One of the hyperpolarisation methods is *parahydrogen* induced polarisation, which uses an iridium catalyst and *parahydrogen* dissolved in the sample. This method enables the detection of signals with up to a thousand-fold increase in sensitivity.

However, sometimes this is still not enough. Some additional signal intensity generated by hyperpolarisation is lost. I predict that it could be lost due to the relaxation of the iridium catalyst. It can potentially be prolonged by the substitution of deuterium for the catalyst ligand and/or co-substrate hydrogens. A slower relaxation process is expected to contribute to further amplification of the signal.

The aim of this work is to determine whether deuteration prolongs relaxation sufficiently to provide additional hyperpolarisation signal enhancement. Based on this, purpose of the work is to create easy to use and reliable method to detect biologically relevant analytes from blood in the lower magnetic field.

1. NMR spectroscopy

1.1 Physical background

1.1.1 Atoms and their parameters in NMR

Most of chemical elements have at least one naturally occurring magnetic isotope. Each of those isotopes magnetic nuclei has spin, an internal angular momentum, which is described by the spin quantum number I . [1] It can have natural number (including zero) and half number values up to $\pm\frac{9}{2}$ [1, 2]. One element's isotopes can have different spin quantum numbers [1]. Particles with integer spin are called bosons and with half-integer spin fermions [3].

Spin angular momentum is a vector I with quantified direction and magnitude. I has a length of $\sqrt{I(I+1)}\hbar$, where $\hbar = \frac{h}{2\pi}$ and h is the Planck's constant. [1] Spin angular momentum has $2I + 1$ allowed projections onto an arbitrarily chosen axis, labelled z , which are degenerate in the absence of external field [1, 3]. In that case, all of those $2I + 1$ projections are equally possible and with the same energy [1].

However, if a magnetic or electric field is applied, they may have different energies [3]. Magnetic energy of a small object depends on the magnetic moment μ and magnetic field B interaction:

$$E = -\mu \cdot B. \quad (1.1)$$

Magnetic energy is lowest if $\mu \parallel B$, which is indicated in the Equation 1.1 by minus sign. [3] In the presence of a strong magnetic field the spin quantisation axis (z) coincides with the field direction. Meaning that Equation 1.1 can be written as

$$E = -\mu_z B. \quad (1.2)$$

In the presence of a magnetic field, each energy level is divided into substates of equal energy. These substates are defined by their angular momentum, and this phenomenon is known as the Zeeman effect (see Figure 1). [4] NMR spectroscopy exploits this effect, focusing specifically on the sublevels of nuclear Zeeman energy states [3].

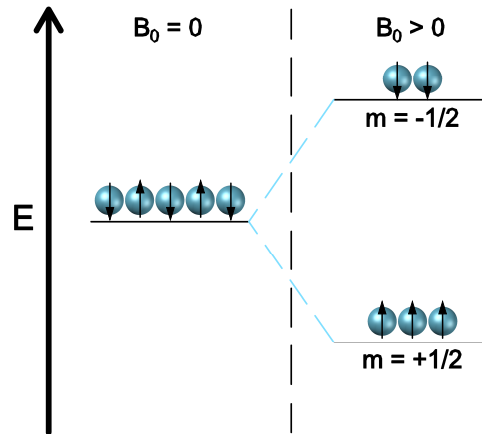


Figure 1. Zeeman splitting.

Some of the nuclear isotopes have zero nuclear spin in the ground state and also show no nuclear Zeeman effect. Therefore, they cannot be measured with NMR spectroscopy as they do not appear in the spectra. Most common ones are ^{12}C , ^{16}O and ^{32}S . [3]

Magnetic moment μ of a nucleus is related to angular momentum I by

$$\mu = \gamma I, \quad (1.3)$$

where γ is a constant called gyromagnetic ratio [1]. It is nucleus specific. In Table 1 are most commonly used nuclei and their spins, gyromagnetic ratios, NMR frequency in 18.8 T field and their natural abundance. Positive or negative sign of the gyromagnetic ratio comes from energy level distributions.

Table 1. Commonly used nuclei and their spins, gyromagnetic ratios, NMR frequency in 18.8 T field and their natural abundance [1, 2, 3].

Nucleus	Spin	$\gamma/2\pi$ (MHz/T)	$ \nu_{\text{NMR}} $ (MHz)	Natural abundance (%)
^1H	0.5	42.58	800	99.99
^2H	1.0	6.54	123	0.01
^{13}C	0.5	10.71	201	1.07
^{14}N	1.0	3.08	58	99.63
^{15}N	0.5	-4.32	81	0.37
^{17}O	2.5	-5.77	109	0.04
^{19}F	0.5	40.08	754	100
^{31}P	0.5	17.25	324	100

By combining Equations 1.2 and 1.3, the amount by which the energy of the nucleus is shifted due to a magnetic field is

$$E = -\gamma I_z B = -m\hbar\gamma B, \quad (1.4)$$

where m is magnetic quantum number. The $2I + 1$ energy levels of spin- I are equally spaced. The selection rule of NMR spectroscopy allows transitions only between neighboring energy

levels, meaning $\Delta m = \pm 1$. Thus the resonance condition is

$$\Delta E = \hbar|\gamma|B \quad (1.5)$$

and resonance frequency is

$$\nu_{\text{NMR}} = \frac{\Delta E}{h} = \frac{|\gamma|B}{2\pi} \quad (1.6)$$

or

$$\omega_{\text{NMR}} = |\gamma|B, \quad (1.7)$$

where h is Planck' constant, ν is frequency and ω is angular frequency [1]. NMR magnets are most commonly referred according to their absolute ^1H frequency value, meaning resonance frequency, which can be calculated with Equation 1.6. It means that a 18.8 T magnet is called a 800 MHz magnet.

Magnetic momentum of a nucleus points in the same direction as spin polarisation ($\gamma > 0$) or in the opposite direction ($\gamma < 0$). From the classical mechanics aspect, when magnetic field is suddenly applied to the sample, spin can be seen as a vector which precesses around the magnet field vector with magnetic moment μ . [3] To be more precise, it is called the Larmour precession and the frequency of this motion is known as Larmour frequency

$$\omega_0 = -\gamma B. \quad (1.8)$$

Precession means that magnetic moment of the spin moves on a cone with constant angle between the spin magnetic moment and the field (see Figure 2). [1, 3] The spinning angle depends only on the initial spin polarisation. [3]

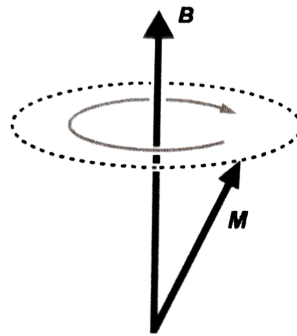


Figure 2. Larmour precession around the magnetic field B with magnetic moment μ . [1]

Coming back to energy levels. Populations of the energy levels of identical, non-interacting spins in a magnetic field are given by Boltzmann distribution at thermal equilibrium. Consider ^1H nuclei in a 18.8 T field at a temperature $T = 298$ K. If α and β represent lower and upper energy levels respectively, the ratio of populations is

$$\frac{\mu_\beta}{\mu_\alpha} = \exp\left(-\frac{\Delta E}{k_B T}\right), \quad (1.9)$$

where $\Delta E = \hbar |\gamma| B$ and k_B is Boltzmann's constant. Evaluating this expression with previously given numbers, $\Delta E = 5.30 \times 10^{-25}$ J, $k_B T = 4.11 \times 10^{-21}$ meaning $\frac{\Delta E}{k_B T} = 1.29 \times 10^{-4}$. For such small values Equation 1.9 can be simplified by using $\exp(-x) \approx 1 - x$ to obtain the relative population difference, named also as polarisation

$$p = \frac{\mu_\alpha - \mu_\beta}{\mu_\alpha + \mu_\beta} \approx -\frac{\Delta E}{2k_B T}. \quad (1.10)$$

With previous numbers, Equation 1.10 gives $p = 6.45 \times 10^{-5}$. It means that from one million of ^1H spins, lower energy level α has only 64 more spins. This is a small excess of spins in the lower energy level. Polarisation is even smaller with weaker magnetic fields or for spins with smaller absolute gyromagnetic ratios, which means for most of the nuclei. [1]

An electromagnetic field excites nuclei from the lower energy level to the upper one with the same probability as it induces the reverse transition. Therefore, the net absorption of energy, and consequently the intensity of the spectroscopic transition, depends on the difference in populations of ground and excited levels. In NMR spectroscopy the upward transitions outnumber downward transitions once per 10^4 - 10^6 transitions. [1] It means that NMR sensitivity is weak. Due to the Equations 1.9 and 1.10 NMR spectroscopy uses high magnetic fields and ^1H is the most sensitive nucleus.

1.1.2 Chemical shift

Although in the Table 1 are given some isotopes, for example ^1H and ^{13}C NMR frequencies, not all of them will have identical resonance frequencies. Exact ν_{NMR} depends on the local electron distribution in the molecule. This effect is called the chemical shift. [1]

Chemical shifts appear in the NMR spectrum because the magnetic field B that nucleus experiences in atom or molecule is slightly different from the magnet produced external field B_0 . B_0 is the field that bare nucleus would feel. B is usually a bit smaller than B_0 because the external field causes electrons to circulate within their atomic orbitals, which induces motion that generates a small magnetic field B' in the opposite direction to the external field:

$$B = B_0 - B'. \quad (1.11)$$

This effect is called shielding as the electrons protect the nucleus from external field. Even so B' is typically 10^4 - 10^5 times smaller than B_0 . Despite that, B' is proportional to B_0 . Therefore, Equation 1.11 can be written as

$$B = B_0(1 - \sigma), \quad (1.12)$$

where σ is proportionality constant between B' and B_0 and is called the shielding constant. The greater shielding, the smaller the chemical shift. As a result resonance condition from Equation 1.6 becomes

$$\omega_{\text{NMR}} = -|\gamma| B_0(1 - \sigma) \quad (1.13)$$

and Larmour frequency Equation 1.8 takes the form of

$$\omega_0 = -\gamma B_0(1 - \sigma). \quad (1.14)$$

To put it another way, the resonance frequency of a nucleus in an atom is a little lower than resonance frequency of a bare nucleus without its electrons. [1]

Previously was said that usually $B < B_0$, because molecules electron configuration might be complicated and result in enlarging external field, not diminishing it. In contrast, it is still named as nuclear shielding. Nucleus resonance frequency is characteristic to its environment as the size and sign of the shielding constant is determined by the electronic structure of the molecule in the neighborhood of the nucleus. [1]

Absolute chemical shifts are used on rare occasions. Hence, it is common practice to define the chemical shift in terms of the difference between the Larmour frequency of the nucleus of interest (ω_0) and that of a reference nucleus ($\omega_{0,\text{ref}}$) using the dimensionless parameter δ :

$$\delta = 10^6 \left(\frac{\omega_0 - \omega_{0,\text{ref}}}{\omega_{0,\text{ref}}} \right). \quad (1.15)$$

δ is independent of the strength of the magnetic field, which makes it easy to compare measurements from different NMR spectrometers. δ values are in parts per million, or shortly ppm. [1] There is an agreement for the zero-point of chemical shift of ^1H and ^{13}C . They are tetramethylsilane ($\text{Si}(\text{CH}_3)_4$), also known as TMS, CH_3 nuclei chemical shifts [5].

NMR spectrum contains additional information in the signal splittings. They appear due to the magnetic interactions between nuclei, known as J-coupling, spin-spin coupling or scalar coupling. [1] Their presence gives rise to multiplets in the spectrum. If two spin-half nuclei are coupled, the resonance from each spin splits symmetrically about the chemical shift into two lines, referred to doublet. [3]

Peaks in the doublet are split by the same quantity, called J-coupling constant. In addition to that, coupling constants are field independent, meaning that they are always the same, no matter of the field strength. Therefore, they are always in Hz. [3]

1.1.3 Fourier transformation

NMR experiment has three main conditions: strong magnetic field to polarise spins, radio frequency pulses to excite the spins and tools to detect NMR signal [1]. It can be done by NMR spectrometer, which is a device that generates magnetisation from nuclear spins with the support of a strong magnetic field, turns magnetisation vector of the nuclei with radio frequency pulse to the xy -plane and measures the rotating spin magnetisation generated oscillating electric current [6].

Detected NMR signal is called a free induction decay (FID). It can be rephrased as following: free of the influence of the radio frequency field, induced in the coil, decaying back to the equilibrium. [7] FID is a time-domain signal, which is, in most cases, uninterpretable by eye. A mathematical procedure, Fourier transform must be implemented to get the so called normal spectrum, frequency-domain signal. [8]

At first Fourier transform multiplies the FID by trial cosine function of known frequency. Resulting in a product function. The area under that product function corresponds to the intensity in the spectrum at the frequency of cosine wave. For more complex cases, it can be combination of cosine waves. Example with three cases is shown in the Figure 3.

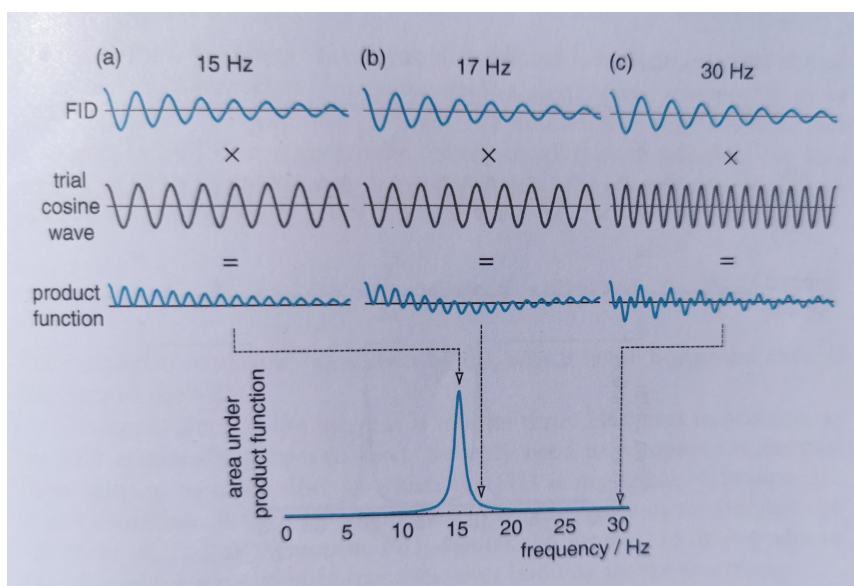


Figure 3. Illustration showing how the Fourier transform works. [8]

In the first scenario (a) in the Figure 3, the trial cosine is at 15 Hz which matches the oscillation in the FID. As a result the product function is always positive, which means that the area under it is a maximum. In second case (b) the trial frequency is 17 Hz. The product function exhibits both positive and negative excursions, but on account of the decay of the FID, the area under the trial function is positive. Nevertheless, it is smaller than the area in case (a). Therefore, the intensity of the spectrum is also smaller. Lastly, in scenario (c) the trial frequency is 30 Hz, which means that the product function oscillates rapidly around zero, resulting in an area under the curve that is essentially zero. Whole process is repeated with trial cosine waves with different frequencies. The spectrum is produced by plotting the area under the product function against the frequency of the corresponding trial cosine wave. Peak width is defined by the signal decay. The longer is the decay, the narrower peak is gotten. [8]

Fourier transform can be describe mathematically in the following way:

$$S_{\text{spectrum}}(f) = \int_0^{\infty} S_{\text{FID}}(t) \cos(2\pi ft) dt, \quad (1.16)$$

where $S_{\text{spectrum}}(f)$ is spectral intensity at frequency f , $S_{\text{FID}}(t)$ the amplitude of the FID at time t . In spite of integral upper limit being infinity, it is limited to some value as FID eventually decays to zero. [8]

Spectrometer measures signal at regular intervals, not consistently, resulting in FID which is actually set of points. To Fourier transform such data each point in the FID is multiplied by the value of the trial cosine wave computed for the time corresponding to that point. Similarly to FID, the product function is a series of data points. After performing the summation, the spectrum reveals the intensity corresponding to the frequency of the trial cosine wave. Therefore in practice, the Equation 1.16 takes the form of

$$S_{\text{spectrum}}(f) = \sum_{i=1}^N S_{\text{FID}}(t_i) \cos(2\pi ft_i). \quad (1.17)$$

S_{FID} is the value at t_i , which the time corresponding to the i th data point from total number on N data points. [8]

To sum up, the Fourier transform is combination of two ideas. Firstly, any time-domain function can be represented by the sum of cosine waves of different frequencies and amplitudes. The number of cosine waves needed depends on the complexity of the measured time-domain function. The frequency-domain function is a plot of the amplitude of these cosine waves as a function of their frequency. Secondly, these cosine waves are orthogonal to each other. It means that the integral of the product of any two cosine waves at different frequencies taken between $t = 0$ and $t = \infty$ is zero. For this reason the integral of Equation 3 is able to pick out contribution at just one frequency. [8]

1.1.4 Relaxation

Relaxation shows how the bulk magnetisation from the spin reaches its equilibrium value over time. NMR relaxation is slow. From the positive aspect, it allows manipulation and observations of any transverse magnetisation that is produced as it survives long enough. Therefore, it is possible to use sequences of pulses and delays that last multiple milliseconds. On the other hand, slow relaxation sets the limit on the rate at which an experiment can be repeated. In order to improve the signal-to-noise ratio, the experiment can be repeated. However, the equilibrium magnetisation must be re-established for that. If the next experiment were to be done before reaching the equilibrium, both the z -magnetisation and the observed signal would be reduced in size. [8]

1.1.4.1 Longitudinal magnetisation and relaxation

For this subchapter used material is from [3]. As previously mentioned in the absence of an external magnetic field, the spin polarisations are uniformly distributed, meaning they are pointing in all possible directions in space. The total magnetic moment of the sample is nearly zero, as there is an approximately equal number of spins pointing in the opposite directions.

When a magnetic field is abruptly applied, all proton spins start undergoing Larmor precession around the field. To provide a specific example, if the external field is 18.8 T, the proton Larmor frequency is $\omega_0 \approx -800$ MHz. Each proton spin completes 800 million full cycles of precession every second.

This precessional motion does not alter the overall magnetic moment of the sample, it is essentially invisible, because of the isotropic distribution of spin polarisations. Although, the proton spins are surrounded by other molecules, which carry also protons, and they are constantly in vigorous motion. The spatial orientation of each molecule undergoes constant changes, and the positions of the molecules relative to each other continuously interchange.

However, to a very good approximation, each nuclear spin is unaffected by its immediate environment. In the presence of a magnetic field, the spin polarisation vectors steadily precess around the magnetic field. It is independent of the fact that they are carried within molecules that undergo rapid rotations and collisions.

Nevertheless, upon closer examination, it is evident that the dynamic molecular environment does have a slight influence on the nuclear magnets. Each molecule contains magnetic particles, including electrons and nuclei, which generate magnetic fields. Although these fields are small, they fluctuate rapidly due to the thermal motion of the surrounding environment. At any given moment, the spin precesses about a field that is the sum of the static external field and a very small microscopic field, which varies in strength and direction in time. Therefore, the local magnetic field experienced by each nuclear spin varies slightly in magnitude and direction compared to its neighboring spins.

However, these variations are very small. For instance, in a water sample with protons subjected to a 800 MHz magnetic field, the fluctuation in the direction of the local magnetic field at the nuclei is approximately only 10^{-4} degrees. Nonetheless, these fluctuations play a significant role in breaking the isotropy of nuclear spin polarisation over time, resulting in the development the emergence of a macroscopic nuclear magnetic moment. In the absence of fluctuating molecular fields, nuclear magnetism would be unobservable.

It was previously said that the wandering motion is isotropic, however, in reality it is not completely isotropic. Due to the finite temperature of the environment, there is a slight preference for nuclear spins to align with low magnetic energy orientation rather than high magnetic energy. Therefore, the thermal wandering slightly favors spin orientations with

magnetic moments aligned parallel to the magnetic field (see Figure 4). The dominance is as small as one of 10^5 spins would be aligned with the field. The biased wandering motion leads eventually to a thermal equilibrium – a stable anisotropic distribution of nuclear spin polarisations.

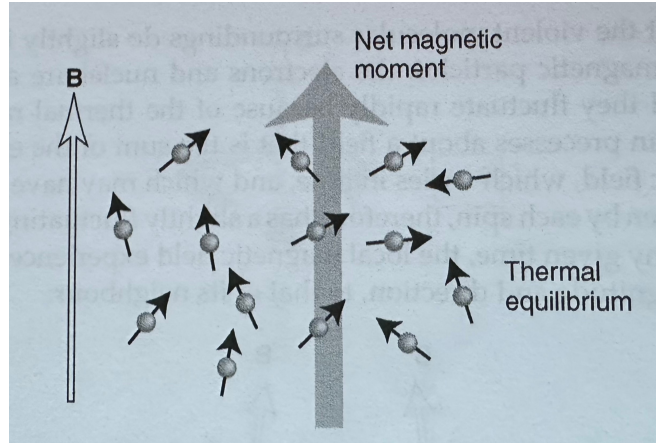


Figure 4. Thermal equilibrium with exaggerated anisotropy for clarity. [3]

The magnetisation distribution in thermal equilibrium is anisotropic, resulting in a small net magnetic moment along the field for the entire sample, referred to as a longitudinal magnetic moment. It is the microscopic mechanism of nuclear magnetism. For protons in water, one can calculate the nuclear contribution to the magnetic susceptibility as follows:

$$\chi_{nuc} = \frac{\mu_0 \hbar^2 \gamma^2 c}{4k_B T} = 4.04 \times 10^{-9}. \quad (1.18)$$

c is the number of protons per unit volume.

When the external magnetic field is abruptly applied or the sample is rapidly exposed to the field, the macroscopic nuclear magnetisation starts from zero and gradually increases over time (see Figure 5). This growth is a result of the biased wandering of spin polarisations, as explained earlier. The build-up curve is typically approximately exponential. If $t_{on} \leq t$ is the moment when the external magnetic field is applied in direction of z -axis, the build-up of longitudinal magnetisation can be expressed as:

$$M_z^{nuc}(t) = M_{eq}^{nuc} \left(1 - \exp\left(-\frac{(t - t_{on})}{T_1}\right) \right). \quad (1.19)$$

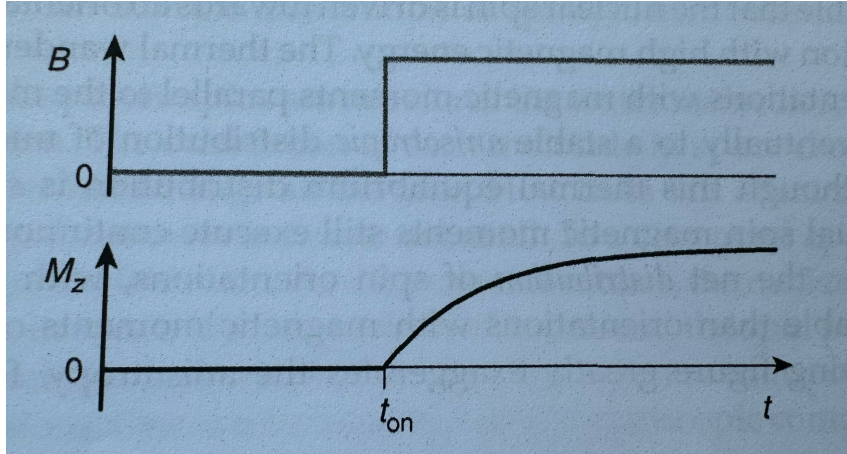


Figure 5. The build-up of longitudinal spin magnetisation before and after the magnetic field is turned on. [3]

The exponential time constant for the process T_1 is known as the spin-lattice relaxation time constant or the longitudinal relaxation time constant. It depends on nuclear isotope and sample, including liquid sample temperature and viscosity.

The term "relaxation" is used to describe the restoration of thermal equilibrium following the application of a perturbation. In the present case, thermal equilibrium is initially achieved without the presence of a magnetic field, resulting in equal probabilities for all nuclear spin orientations. However, with the introduction of a magnetic field, this equilibrium state is disrupted, and the system "relaxes" towards a new equilibrium characterized by an anisotropic distribution of spin polarisations (see also Figure 5). If the magnetic field is suddenly switched off at $t_{\text{off}} \leq t$, the nuclear spin magnetisation relaxes back to zero (see Figure 6). It can be described mathematically by

$$M_z^{\text{nuc}}(t) = M_{\text{eq}}^{\text{nuc}} \left(1 - \exp \frac{-(t - t_{\text{off}})}{T_1} \right). \quad (1.20)$$

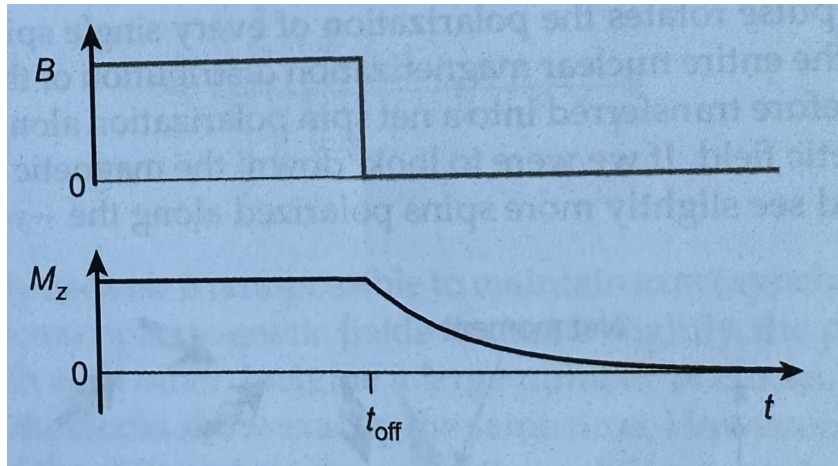


Figure 6. The decay of longitudinal spin magnetisation before and after the magnetic field is turned off. [3]

1.1.4.2 Transverse magnetisation and relaxation

For this subchapter used material is from [3]. The longitudinal nuclear spin magnetisation, as described before, is almost undetectable. It is about four orders of magnitude less than the typical sample diamagnetism, which is associated with the electrons.

NMR spectroscopy employs a different approach by measuring the magnetisation perpendicular to the external magnetic field rather than along it. Suppose that the spin system is allowed to reach thermal equilibrium in a large magnetic field. In this state, the macroscopic nuclear magnetisation aligns along the direction of the external field (the z -axis, by convention) and reaches an equilibrium value M_{eq}^{nuc} .

There is no net magnetisation perpendicular to the field on a microscopic level, because on average, the magnetisation distribution in thermal equilibrium is symmetrical around the z -axis.

Considering a scenario where the polarisation of each individual spin is abruptly rotated by $\frac{\pi}{2}$ radians around the x -axis, induced by a radio frequency pulse. As a result the spin polarisation is along the $-y$ -axis (see Figure 7).

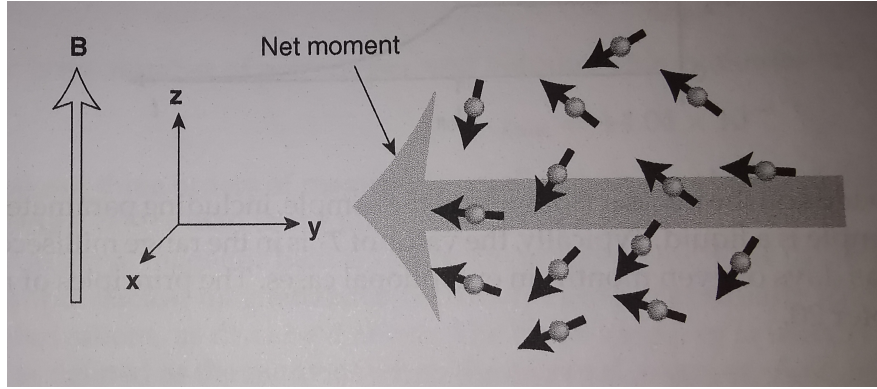


Figure 7. Polarisation distribution after $\frac{\pi}{2}$ pulse around x -axis. [3]

The pulse rotates the entire nuclear magnetisation distribution of the sample among the polarisation of every single spin in the sample by the same angle. The net spin polarisation along the z -axis is therefore transferred into a net spin polarisation along the $-y$ -axis. In other words, it is along an axis perpendicular to the magnetic field. This net magnetic moment is called transverse magnetisation.

When the pulse is deactivated, the spins resume their precessional motion. On a microscopic level, the individual spins precess as usually. On a macroscopic scale, a new phenomenon emerges. Immediately after the pulse, the state of the system exhibits a net polarisation along the $-y$ -axis, which is perpendicular to the main magnetic field. As each individual spin undergoes precession, the net magnetic moment also precesses. The macroscopic nuclear magnetisation rotates in the xy -plane, which is perpendicular to the main magnetic field. The frequency of precession of the transverse magnetic moment is the same as the frequency of precession of the individual spins, known as the nuclear Larmor frequency (see also Equation 1.8).

The macroscopic magnetisation components at a time t after the pulse can be expressed as

$$M_y^{nuc}(t) = -M_{eq}^{nuc} \cos(\omega_0 t) \exp\left(-\frac{t}{T_2}\right), \quad (1.21)$$

$$M_x^{nuc}(t) = M_{eq}^{nuc} \sin(\omega_0 t) \exp\left(-\frac{t}{T_2}\right). \quad (1.22)$$

The transverse magnetic moment undergoes precession at the nuclear Larmor frequency ω_0 , slowly decaying at the same time (see Figure 8).

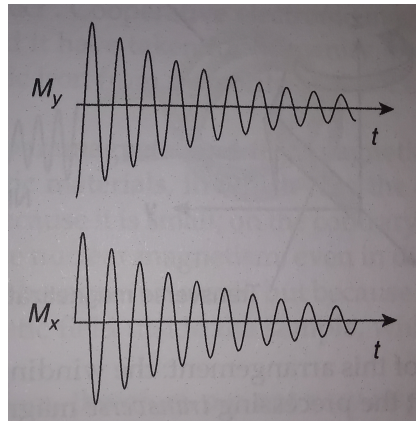


Figure 8. Decay and oscillation of the transverse magnetisation. [3]

The gradual decay of the transverse magnetisation occurs due to the inability to maintain precise synchrony among the precessing nuclear magnets. The microscopic magnetic fields fluctuate slightly, causing the precessing nuclear magnets gradually get out of phase with each other. In other words, destruction of transverse magnetisation requires that different spins experience slightly different magnetic fields, so that they precess at slightly different frequencies. This property holds true in all real samples, regardless of whether there is spin interaction between the nuclei.

The decay of the transverse magnetisation is irreversible, meaning that once it is lost, it cannot be recovered. The precessing nuclear magnets cannot be brought back into phase without repeating the entire experiment. This process is commonly referred to as homogeneous decay. The time constant T_2 , also known as transverse relaxation time constant and spin-spin relaxation time constant, takes into account the homogeneous decay of the precessing macroscopic nuclear magnetisation.

To alter the field direction component, the energy of the sample spin system must change. It can be done with perturbing the spins with a radio frequency pulse. Then the spin system will return to the equilibrium, when there is an interaction between the spins and surroundings, or lattice, leading to a loss of energy. The rate at which the system returns to equilibrium is determined by the interaction's capability to transfer energy to or from the system. Returning to the equilibrium generally occurs with a first-order rate constant R_1 . [7]

Relaxation rate constant depends on the relaxation time constant T_1 as following

$$R_1 = \frac{1}{T_1}.$$

Relaxation time constant is more used to refer to the relaxation as it is commonly studied by time-dependent measurements. To be more precise, R_1 and T_1 are referred to as the spin-lattice relaxation rate and time constant, respectively. All together they can be referred to as longitudinal relaxation components. [7]

In non-equilibrium the magnetisation may have components on xy -plane, which will relax to their equilibrium value, zero (see Figure 6). xy -magnetisation will decay similarly as the z -magnetisation, although, it can be lost by additional processes. By those processes the xy -magnetisation will fan out or dephase, which results in net magnetisation of zero. Relaxation rate and time constant of the xy -plane are respectively R_2 and T_2 . They are also referred to as the spin-spin or transverse relaxation rate and time constants, respectively. Their relation is similar to spin-lattice relaxation constants:

$$R_2 = \frac{1}{T_2}.$$

Additional processes mentioned above do not necessarily require any change in energy, which means that the rate of xy -relaxation may be faster than the longitudinal relaxation. [7] In other words, $R_2 \geq R_1$ or $T_2 \leq T_1$.

Factors contributing to the signal decay may be both intrinsic to the molecules as well as experimental, for example poor shimming of the magnetic field. Therefore, actual rate and time constants of decay seen in the FID are denoted R_2^* and T_2^* respectively, while the R_2 and T_2 are intrinsic relaxation rate and time constants. [7]

1.2 Hyperpolarisation

Nuclear spin hyperpolarisation increases transiently the differences in nuclear spin populations [9]. Therefore, signals can be observed with higher intensity due to signal amplification of hyperpolarisation. The intensity of these signals is typically too low to be detected by conventional methods, but hyperpolarisation techniques can reveal otherwise undetectable signals. In other words, compounds, including contaminations that are not detected in regular ^1H NMR may be seen with hyperpolarisation. There are different hyperpolarisation methods, such as dynamic nuclear polarisation, spin-exchange optical pumping and *parahydrogen* induced polarisation (PHIP) [9]. Non-hydrogenative PHIP (referred to as nh-PHIP) is the hyperpolarisation method that is studied in this paper.

Para- and *ortho*hydrogen are nuclear spin isomers of hydrogen gas, which are also known as a nuclear singlet and a nuclear triplet states, respectively. They differ in the spin alignment of hydrogen nuclei. In *ortho*hydrogen the spins of the two hydrogen nuclei are aligned, while in *parahydrogen*, they are opposed (see Figure 9). Singlet and triplet states are defined as:

$$\begin{aligned} |T_{-1}\rangle &= |\beta\beta\rangle, \\ |T_0\rangle &= \frac{1}{\sqrt{2}}(|\alpha\beta\rangle + |\beta\alpha\rangle), \\ |T_1\rangle &= |\alpha\alpha\rangle, \\ |S_0\rangle &= \frac{1}{\sqrt{2}}(|\alpha\beta\rangle - |\beta\alpha\rangle). \end{aligned} \tag{1.23}$$

At room temperature a volume of hydrogen gas contains 25% *parahydrogen* and 75% *orthohydrogen*. [10, 11] In other words, the population of all four energy levels is roughly equal (see also Figure 10a) and all energy level are almost equally populated according to Boltzmann distribution (see also Figure 10b). However, in a pure *parahydrogen* only one energy state exist, which results in signal enhancement. Only $\alpha\beta$ and $\beta\alpha$ are populated in Figure 10b, which is non-Boltzmann distribution. [11]

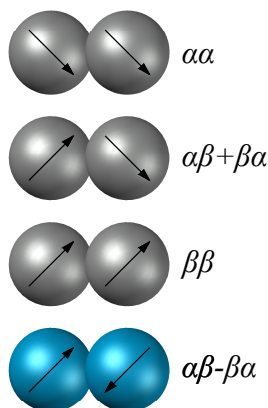


Figure 9. Four spin combinations of H_2 split into two isomers of *ortho*- and *parahydrogen* (grey and blue, respectively). The difference is in the orientation of the nuclei. α and β denote the spin-up and spin-down states of the protons in hydrogen gas, respectively.

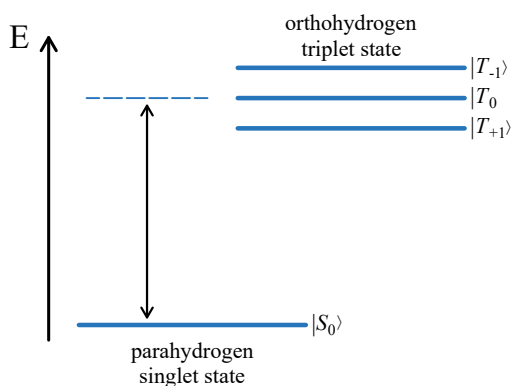


Figure 10. Energy level diagrams for the nuclear spin states of H_2 depicted (a) before and (b) after undergoing a pair-wise hydrogenation reaction that leads to chemical or magnetic inequivalence between the two nuclei. α and β denote the spin-up and spin-down states of the protons in hydrogen gas, respectively. Relationships between the states in (a) and (b) are written in Equations 1.23. [11]

The spin configuration of *parahydrogen* can be converted to spin hyperpolarisation in the transient complex. See also Figure 11, which shows the complexation process of Iridium complex with *parahydrogen* and analyte. This can result in up to thousand times stronger NMR hydride signals. [9]

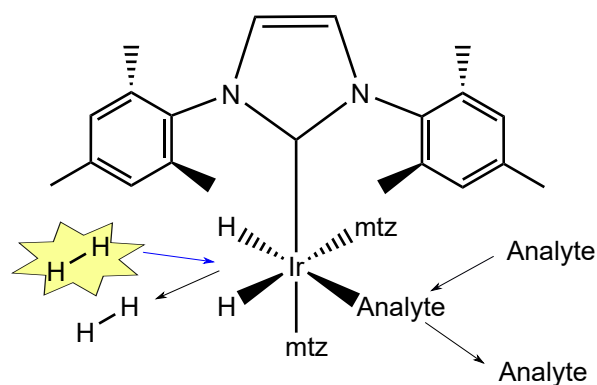


Figure 11. Schematic representation of the *parahydrogen* experiment. $[\text{Ir}(\text{H})_2(\text{IMes})(\text{mtz})_2\text{Analyte}]^+$ with *parahydrogen* and analyte complexation. On the left is shown hydrogen exchange, where *parahydrogen* pair is highlighted, and on right is shown analyte exchange.

Hydrides resonate in a region of the ^1H spectrum that is generally signal-free (around -20 ppm). Therefore, the indirect detection of analytes in a solution offers significant advantages in the case of complex systems. The enhanced sensitivity from nh-PHIP accompanied by the absence of interference from the complex sample matrix (usually between $0-10$ ppm in spectrum) can detect concentrations as low as sub- μM , which is approximately three orders of magnitude lower than for conventional NMR. The issues of signal crowding and NMR sensitivity are tackled collectively. Therefore, nh-PHIP is a powerful tool for NMR analysis of low-concentration compounds in complex mixtures. [9]

2. Blood and diagnostics

Blood is a constantly circulating body fluid. It consists of plasma and blood cells. Blood cells divide into three: red blood cells (RBCs), white blood cells (WBCs) and platelets. Plasma is the liquid component of blood, which is a mixture of water, sugar, fat, protein and salts. Its main task is to transport substances, including blood cells, through the body. Plasma contains also clotting proteins, so it helps blood to clot. RBCs, which are also called erythrocytes, contain protein called hemoglobin with which RBCs carry oxygen to the tissues. WBCs, which are also called leukocytes, protect the body from infection. WBCs divide into different types, depending on their exact protection mechanism. Third part of the blood cells, platelets, also called thrombocytes, help blood to clot by forming a platform on which blood coagulation can occur. [12, 13]

Human plasma is considered the most important and one of the most convenient sources of circulating biomarkers, because plasma is designed to carry nutrients, electrolytes, proteins, hormones, nitrogenous waste and dissolved gases to the different parts of the body [14, 15]. In addition to its beneficial components, blood also carries harmful substances. Therefore, biomarkers can provide valuable information about the physiological and pathological conditions of an individual. Plasma can be obtained through a relatively non-invasive procedure, blood draw. [14]

Blood tests are common practice of health care. They preserve high value in diagnostics, monitoring treatment effectiveness and overall well-being. One of the blood test is the basic metabolic panel, which is also a group of tests. It measures various naturally occurring chemicals present in the blood in order to provide information about health of organs. Typically, these tests are performed on plasma. [16]

It has shown that plasma provides a stable matrix for the detection of analytes and biomarkers susceptible to hemo- and leukolysis. It is one of the reasons why basic metabolic panel blood test is also done on the plasma. Therefore, development of blood POC testing methods include also plasma extraction. [14]

3. Energy metabolism of cancerous cells

Cell is the smallest unit of life. All living organism are made up from them. Cells must regulate and coordinate common and cell specific processes and functions. Loss of control may end up with severe consequences, the development of cancer. [17]

Cell homeostasis is regulated by cell division, growth arrest and death. Cell division, which is regulated by numerous proteins, is the process wherein a parent cell divides into daughter cells. Special proteins will stop the growth. Turnaround in these processes cause inappropriate and unregulated cell division which is one of the causes of cancer.[17]

There are two types of cell death mechanisms. Cells can die by a lethal injury or apoptosis. First one can occur after lack of oxygen, essential nutrients, exposure to extreme temperature or a traumatic injury. Second, apoptosis, is an internally programmed cell death. It is important in a variety of physiologic and pathologic conditions. It eliminates cells during development. Furthermore, apoptosis exterminates precancerous and virus-infected cell. Nevertheless, some cancer cells manage to escape from it. Abnormal resistance to apoptosis is characteristic of most cancers. [17]

Major modifications between normal and malignant cells appear in energy metabolism, particularly in use of glucose. The most efficient energy production process in cells is carried out by glycolysis in the tricarboxylic acid cycle, where 36 adenosine triphosphate (ATP) molecules are produced for each glucose molecule. This metabolism is carried out by oxygen use and is the main pathway for energy production in the majority of cells. [18]

ATP is a molecule consisting adenine, ribose sugar and three phosphate groups (see Figure 12a) [19]. It carries energy within cells and fuels energy dependent biochemical processes [19, 20]. Adenosine diphosphate (ADP) differs from ATP by having one phosphate group less (see Figure 12b). Adenosine monophosphate (AMP) is similar to ATP and ADP, but has only one phosphate group (see Figure 12c). [19] As ADP and AMP are closely associated with ATP, the levels of all three represent a measure of the energetics of the functioning cells and their mitochondria [20]. In animal and plant cells the key parameters of regulating metabolism and respiration are ATP/ADP ratio and energy charge [21].

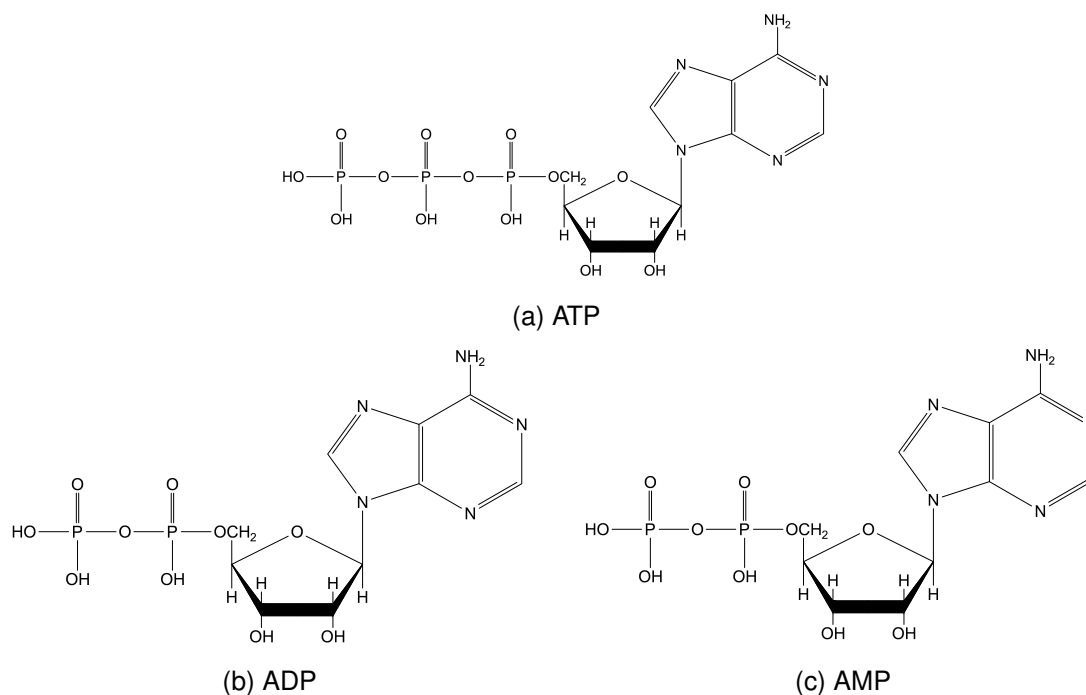


Figure 12. Molecule structures of ATP, ADP and AMP.

Cancer hallmark is the ability to reprogram energy metabolism to support malignant cell proliferation and metastatic activity. However, the molecular mechanisms and logic of such metabolic rearrangements and adjustments are still mostly unknown. The connection between mitochondrial ATP production and the sites of ATP utilization in various cellular compartments to promote the growth of malignant cells is still unclear. [22]

The metabolic hybrid phenotype of cancer is one of the reasons why malignant cells incline to metastasis and are cancer therapy resistant [22, 23]. It has been found that in most tumors, mitochondria are not defective in their ability to carry out oxidative phosphorylation (OXPHOS) [23]. OXPHOS is a cellular process that harnesses the reduction of oxygen to generate high-energy phosphate bonds in the form of ATP [24].

Opposed to normal cells, in hybrid metabolic state glycolysis and OXPHOS are simultaneously active. A study of Klepinin et al. of triple-negative breast cancer (TNBC) showed that intracellular ATP levels increased in cancer cells. In addition to that, ATP and ADP ratio considerably decreased. In TNBC cells, it has been observed that 70% of the ATP is produced through the glycolytic pathway, indicating a metabolic shift as compared to control cells, where OXPHOS is the main provider of ATP. [22]

In addition to that, there is a hypothesis that ATP levels increase in plasma due to the direct action of extracellular ATP on the tumor and host tissues [25]. Accurate and efficient measurement of co-enzymes involved in redox reactions and energy is crucial for studying and gaining insights into the mechanisms underlying both normal and impaired cellular functions [20].

4. Aims of the present work

Intensity of hyperpolarised signals in nh-PHIP chemosensing are the result of a chemical (analyte and *parahydrogen* exchange) and nuclear relaxation process on the iridium catalyst. This work investigates the impact of nh-PHIP catalyst ^2H -labeling on the dipolar relaxation within the analyte-catalyst complex and on the intensity of hyperpolarised chemosensor signals.

- Determine the effect of ^2H -labelling in nh-PHIP catalyst complex on hydride signals of biologically relevant analytes (adenosine and nicotinamide), by measuring the T_1 and T_2 relaxation time constants.
- Determine the effect of ^2H -labelling of N-heterocyclic carbene ligand on nh-PHIP signals.
- Determine the effect of ^2H -labelling of co-substrate on nh-PHIP signals.
- Determine the effect of temperature and magnetic field on T_1 and T_2 relaxation time constants.
- Apply the optimised conditions in nh-PHIP analysis of human blood to detect ATP, ADP and AMP for potential application in cancer diagnostics.

5. Method development

5.1 Technical details

5.1.1 NMR spectrometers and used equipment

Most of the NMR experiments were performed on a Bruker Avance III 800 MHz (18.8 T) spectrometer equipped with TXI, BBO or cryogenically cooled probes. Lower field experiments were done on a Bruker Avance III 400 MHz (9.4 T) spectrometer with BBO probe and Bruker Avance II 200 MHz (4.7 T) spectrometer with QNP probe. Some measurements were done on Agilent DD2 500 MHz (11.74 T) spectrometer with BBO probe. Unless it is specified, Bruker 800 MHz spectrometer and TXI probe were used.

Scale, automatic pipettes and pH-meter were used for sample making. Components that required weighting were weighted using Sartorius analytical scale MSY (SJ EG) with 10^{-6} g accuracy. BRAND Transferpette S (100–1000 μ l), BRAND Transferpette S (10–100 μ l) and Biohit M200 (20–200 μ l) automatic pipettes were used. pH was measured with Laboratorní přístroj MM 2A pH-meter.

Samples preparation steps were made into 1.5 and 2 ml Ependorffes. They were stirred with Biosan Vortex V-1plus stirrer and in the Bandelin Sonorex Digitech UV-bath. To separate solid parts from the solution, MPW-310 centrifuge was used.

Samples were measured with Boroeco-5-7 5 mm NMR tubes, 3 mm NMR tubes and 5 mm medium wall Wilmad® quick pressure valve NMR tube.

Measurements were analysed with Bruker TopSpin 3.6.4 and MestreNova 14.3.1 programs. Relaxation was calculated by choosing the areas in TopSpin and using the T_1/T_2 relaxation calculating submodule in TopSpin dynamics analysing module. T_1 and T_2 measurements were done with separate pulse programs. Depending on the measurement, program gave out corresponding relaxation information.

5.1.2 Reagents and stock solutions

Chemicals

Na_2HPO_4 , NaH_2PO_4 , ethylenediaminetetraacetic acid disodium salt dihydrate, Chelex 100 Resin, adenosine-5'-triphosphate disodium salt hydrate, adenosine-5'-diphosphate sodium salt, adenosine-5'-monophosphate sodium salt, 3-(trimethylsilyl)propionic-2,2,3,3- d_4 acid sodium salt, MgCl_2 , CD_3OD , D_2O were purchased from common international chemical suppliers and used as supplied. The iridium catalyst complex precursors $[\text{Ir}(\text{Cl})(\text{COD})(\text{IMes})]$ and $[\text{Ir}(\text{Cl})(\text{COD})(\text{IMes-}d_{22})]$ (COD: cyclooctadiene, IMes: 1,3-bis(2,4,6-trimethylphenyl)-imidazole-2-ylidene) was prepared according to published methods [26, 27]. 1-methyl-1,2,3-triazole (mtz) and mtz- d_5 was synthesized based on a published procedure [28] at -21°C and purified by vacuum distillation.

Phosphate buffer Phosphate buffer was made according to article [29] with 12.07 mg of Na_2HPO_4 , 2.63 mg of NaH_2PO_4 and 1008.51 mg of D_2O , which were weighted and mixed together. pH of the buffer was 7.51.

EDTA solutions

0.1 M EDTA solution in NaOH was made by dissolving 7.306 mg of Na_2EDTA in 1M NaOH, which was made by dissolving 0.6 g of NaOH in 15 ml of H_2O . pH of EDTA solution was 11.3.

2.9 M EDTA solution in CD_3OD and NaOH (for dissolving properties) was made by dissolving 1.159 mg of EDTA in 1.322 ml of CD_3OD and 40.6 μl of NaOH.

AMP, ADP and ATP solutions with Mg^{2+}

0.264 mg of MgCl_2 and 0.962 mg of AMP were dissolved in 0.554 ml of distilled water. NaOH and HCl were added to raise pH from 5.58 to 8.76. As a result 5 mM AMP solution with Mg^{2+} was obtained.

5.677 mg of ADP was dissolved in distilled water, 10 mM MgCl_2 solution, which was made by dissolving 9.705 mg of MgCl_2 in 0.204 ml of distilled water. NaOH and HCl were added to raise pH from 4.08 to 8.58. pH was raised in two stages. Firstly, only for ADP solution up to pH 7, after which was MgCl_2 solution added and pH raised to desired value. As a result 10 mM ADP solution with Mg^{2+} was obtained.

5.527 mg of ATP was dissolved in distilled water and 10 mM MgCl_2 solution, which was made by dissolving 9.705 mg of MgCl_2 in 0.204 ml of distilled water. NaOH and HCl were added to raise pH from 3.31 to 8.68. pH was raised in two stages. Firstly, only for ADP solution up to pH 7, after which MgCl_2 solution was added and pH raised to desired value. As a result 10

mM ATP solution with Mg^{2+} was obtained.

5.1.3 Sample preparation for NMR experiments

Base chemical compounds for nh-PHIP experiments were catalyst precursor $[Ir(Cl)(COD)(IMes)]$, also known as N-heterocyclic carbene ligand, and 1-methyl-1,2,3-triazole, which is called co-substrate. All of the catalyst precursor and co-substrate solutions were made in deuterated methanol (CD_3OD). Catalyst precursor is referred to as IMes and co-substrate as mtz henceforward.

Solutions of IMes and mtz were measured by volume into a NMR tube. NMR tube containing IMes, mtz and CD_3OD was then pressurised under 5 atm of H_2 , shaken and allowed to hydrogenate at room temperature for two hours. Which resulted in a solution of the active $[Ir(H)_2(IMes)(mtz)_3]^+$ catalyst. It is referred to as iridium complex henceforward. After the iridium complex was formed chemical background measurements were done.

Preliminary temperature experiment

NMR tube contained 1.2 mM IMes, 76.7 mM mtz, 0.1 mM adenosine (molecule structure in Figure 13a) and 0.1 mM nicotinamide (molecule structure in Figure 13b), last two were added as analytes. Total sample volume was 600 μ l.

To ensure that the analytes would go to only position showed in Figure 11, mtz is added intentionally in excessive amount and analyte is added in sub-micromolar amounts. If the co-substrate mtz is present at a higher concentration than the catalyst precursor, it minimizes the formation of mixed complexes and only complexes shown in Figure 11 form [9].

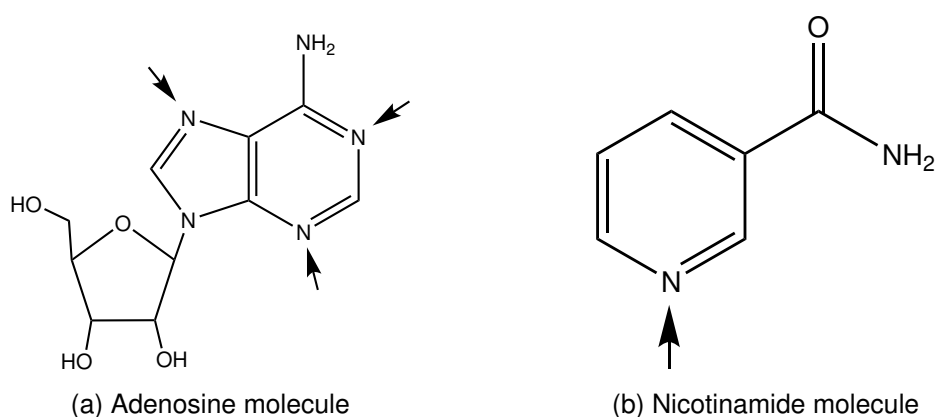


Figure 13. Used analytes and their possible binding sites with iridium complex indicated with arrows (based on work by Wood *et al* [30]). In nh-PHIP experiments adenosine binds from only two positions out of three.

T₁ and T₂ relaxation time constant experiments

Different combinations of unlabelled and ^2H -labelled catalyst precursor with unlabelled and ^2H -labelled co-substrate were made by activating desired combinations in NMR tube. Therefore, following combinations formed: unlabelled catalyst precursor with unlabelled co-substrate ($[\text{Ir}(\text{H})_2(\text{IMes})(\text{mtz})_3]^+$), unlabelled catalyst precursor with ^2H -labelled co-substrate ($[\text{Ir}(\text{H})_2(\text{IMes})(\text{mtz-d}_5)_3]^+$), ^2H -labelled catalyst precursor with unlabelled co-substrate ($[\text{Ir}(\text{H})_2(\text{IMes-d}_{22})(\text{mtz})_3]^+$) and ^2H -labelled catalyst precursor with ^2H -labelled co-substrate ($[\text{Ir}(\text{H})_2(\text{IMes-d}_{22})(\text{mtz-d}_5)_3]^+$).

NMR tube contained 1.2 mM $[\text{Ir}(\text{Cl})(\text{COD})(\text{IMes})]$ or $[\text{Ir}(\text{Cl})(\text{COD})(\text{IMes-d}_{22})]$, 76.7 mM mtz or mtz-d₅, 0.07 mM adenosine and 0.1 mM nicotinamide with a total sample volume of 600 μl .

Blood sample preparation

Human whole blood from healthy individuals were obtained from The North Estonia Medical Centre. Whole blood extracts were prepared by a supervisor according to article [29]. Whole blood extracts were collected in heparinized blood collection tubes.

Blood sample preparation was done by supervisor. Extraction method used 400 μl of whole blood. The biospecimens were mixed with methanol and chloroform in a 1:2:2 volume ratio. After that the solutions were vortexed for 30 seconds, sonicated for 2 minutes at 4°C, and incubated at -20°C for 20 minutes. Acquired mixtures were centrifuged at 13 400 rcf for 30 min to pellet proteins and cell debris. Clear aqueous solutions were transferred to fresh vials. Organic solvents (chloroform and methanol) were blown away with nitrogen and leftover dried in lyophilisator for 5 hours. Dried samples were stored in -80°C fridge until used in experiments. In that temperature there is no biological activity, meaning that samples do not change in biochemical composition. Those samples are referred to as whole blood extracts.

Whole blood extract preparation without additional treatment

IMes and co-substrate were dissolved in CD_3OD . Whole blood extract was lyophilised after which dissolved in 800 μl of degassed CD_3OD . NMR tube contained 200 μl of this solution, 1.2 mM of IMes and 21.7 mM (in other words 18-fold excess) of mtz. This sample was made and measured by supervisor.

ATP, ADP and AMP sample preparation with Mg^{2+}

IMes, mtz, nicotinamide and corresponding phosphate (ATP, ADP or AMP) solution with Mg^{2+} (see Chapter 5.1.2) were dissolved in CD_3OD . The nh-PHIP sample consisted of 1.2 mM IMes, 18-fold excess of mtz, 0.1 mM nicotinamide and, depending on the measurement, 0.02, 0.10 or 0.30 mM of AMP, ADP or ATP with Mg^{2+} with a total sample volume of 600 μl . Samples had maximum 6% of water.

ATP, ADP and AMP sodium salts sample preparation

IMes, mtz, nicotinamide and corresponding phosphate (ATP, ADP or AMP) were dissolved in CD₃OD. The nh-PHIP sample consisted of 1.2 mM IMes, 18-fold excess of mtz, 0.2 mM nicotinamide and, depending on the measurement, 0.1 mM of AMP, ADP or ATP with a total sample volume of 600 µl. These samples were made and measured by supervisor.

ATP nh-PHIP signal enhancement by 2H-labelled iridium complex sample preparation

ATP sodium salt, adenosine and nicotinamide were dissolved in CD₃OD. The nh-PHIP sample consisted 1.2 mM of catalyst precursor, 18-fold excess of co-substrate, 0.1 mM of ATP, 0.1 mM nicotinamide and 0.07 mM of adenosine. For one case formed complex was [Ir(H)₂(IMes)(mtz)₂Y]⁺ and for another Ir(H)₂(IMes-d₂₂)(mtz-d₅)₂Y]⁺, where Y marks ATP, nicotinamide or adenosine.

Whole blood extract sample preparation with Chelex

The whole blood extract was lyophilised taken up in 1 ml of distilled water and excess of Chelex was added. The mixture was put into a spinner and stirred for 20 hours at 4°C. The water phase was decanted and lyophilised. 800 µl of CD₃OD was added to the lyophilised sample. The leftover solids were pelleted in the centrifuge.

The nh-PHIP sample consisted of 400 µl of the other half of the clear methanol solution, 1.2 mM IMes and 18-fold excess of mtz with a total sample volume of 600 µl. ¹H and ³¹P spectrum were measured.

The leftover solids were taken up in 200 µl phosphate buffer (see Chapter 5.1.2) and centrifuged after which ¹H and ³¹P were measured.

Whole blood extract in phosphate buffer sample preparation

The whole blood extract was lyophilised and taken up in 200 µl of phosphate buffer (see Chapter 5.1.2). pH of this solution was 7.5. ¹H and ³¹P were measured. This sample was made and measured by supervisor.

Whole blood extract sample preparation with EDTA

The whole blood extract is taken up in 400 µl of distilled water and centrifuged. Sample pH was 8.6. Sample was measured with internal standard insert containing 150 µl 25 µM of 3-(trimethylsilyl)propionic-2,2,3,3-d₄ acid sodium salt in D₂O. Another ¹H and ³¹P were measured from the same sample with 1.8 mM of EDTA with a total sample volume of 400 µl. Sample pH was 11.3. This sample was divided into two by weight. One half was lyophilised

and taken up in 400 μl of CD_3OD . 165 μl of it was additionally diluted in 35 μl of CD_3OD . ^1H and ^{31}P were measured.

Another whole blood extract was melted and part of its water-methanol layer taken and centrifuged. 100 μl of it was diluted in 300 μl of CD_3OD . The nh-PHIP sample consisted of 1.2 mM IMes, 18-fold excess of mtz, 100 μl of whole blood extract water-methanol solution with a total sample volume of 600 μl . Sample had less than 6% of water. Another nh-PHIP sample consisted of 1.2 mM IMes, 18-fold excess of mtz, 100 μl of whole blood extract water-methanol solution and 0.3 mM of EDTA with a total sample volume of 600 μl . Sample had less than 6% of water. Third nh-PHIP sample consisted of 1.2 mM IMes, 18-fold excess of mtz, 160 μl of previously mixed whole blood extract water-methanol solution (100 μl) and EDTA (0.3 mM final concentration) with a total sample volume of 600 μl . Sample had less than 6% of water. For fourth nh-PHIP sample, another portion of EDTA was added with resulting EDTA final concentration of 0.45 mM.

5.2 Results and discussion

nh-PHIP measurement's spectra were obtained with the spectral window ranging from -12.0 to -32.0 ppm. In the measurements, signals of the analytes appear only in region -19.2 to -23.4 ppm, in most cases -21.2 to -23.4 ppm. One of the typical measurements is shown in Figure 14. nh-PHIP experiment gives signals for adenosine and nicotinamide that are in pairs that have left and right-hand side doublets. They can be affiliated by doing 2D measurement on the sample.

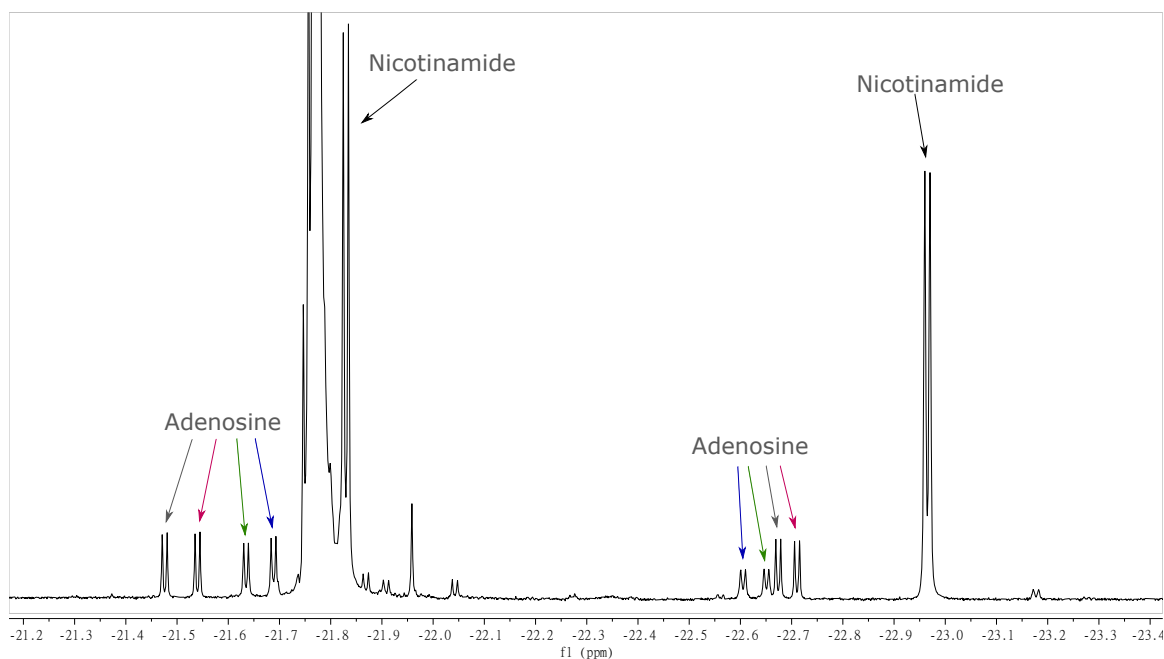


Figure 14. Hyperpolarised 1D spectrum of a adenosine and nicotinamide iridium complexes from -21.2 to -23.4 ppm. Different arrow colours represent doublet pairs.

In Table 2 are adenosine and nicotinamide doublets chemical shifts. Pairs are marked also in Figure 14 and 15 with colours. Pairs were assigned according to 2D ZQ-COSY nh-PHIP measurement (see Figure 15). Between left-hand side adenosine and nicotinamide signals is iridium cosubstrate symmetric complex in large excess in region -21.73...-21.80 ppm. This complex contributes to the intensity of the nicotinamide left-hand side signal. Doublet around -23.17 ppm appears due to the cross-contamination. It does not overlap with analytes under investigation, meaning nicotinamide and adenosine, therefore, its existence can be ignored.

Table 2. Adenosine and nicotinamide iridium complex hydrides' chemical shifts.

Analyte	Chemical shift (ppm)
Adenosine	-21.475 & -22.615
	-21.540 & -22.652
	-21.635 & -22.675
	-21.690 & -22.712
Nicotinamide	-21.830 & -22.965

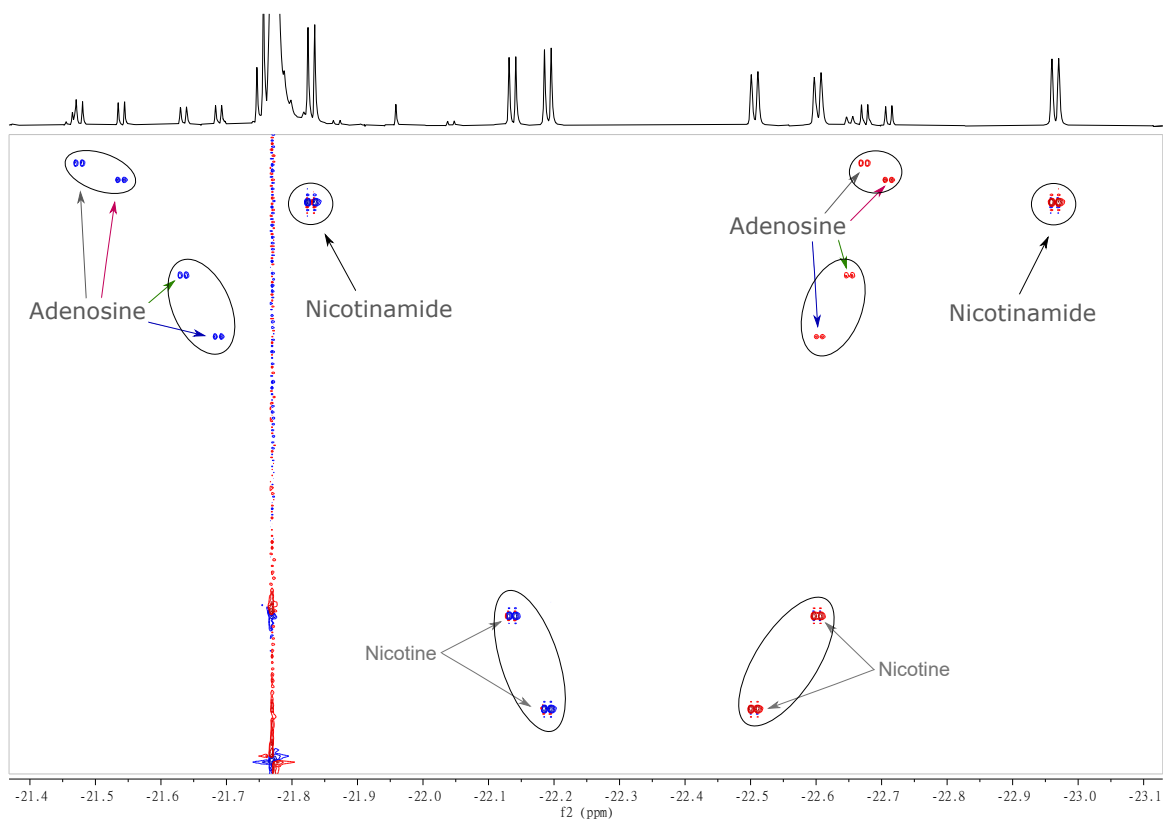


Figure 15. Hyperpolarised 2D measurement of adenosine, nicotinamide and nicotine iridium complexes. Different arrow colours represent doublet pairs as in Figure 14.

Figure 15 also shows signals for nicotine. Nicotine, along with several other analytes, was considered as a potential third analyte. However, it was found to overlap with adenosine signals in the one-dimensional hyperpolarisation spectrum, so it was not included in later experiments. Other analytes (cotinine, 1-methyl-adenosine, pyridine) faced similar issues, as they overlapped with adenosine or nicotinamide signals.

Adenosine is a chiral molecule that has three possible binding sites to form a complex with iridium (see arrows in Figure 13a). When a chiral molecule complexes with a symmetric iridium complex ($[\text{Ir}(\text{IMes})(\text{H})_2(\text{mtz})_3]\text{Cl}$) diastereomers form. In the case of adenosine two diastereomer pairs should form for each of the three binding sites. However, the third binding site is either unused or forms complexes at very low concentrations, making it difficult to observe. Therefore, four pairs of doublets from adenosine appear in the spectrum. The first two on the left (see Figure 14 and Figure 15 upper adenosine signals) are diastereomers, while the other two together form another diastereomer pair (see Figure 14 and Figure 15 lower adenosine signals). Diastereomers are type of stereoisomers, which are sets of molecules that have the same chemical formula, and the same connectivity, but differ in how their atoms are arranged in space and are non-superimposable [31].

Nicotinamide on the other hand has only one hydride pair, because it is not chiral (does not contain chiral centers) and contains only one site that forms a complex with iridium (see arrow in Figure 13b). Therefore, it gives only one pair of doublets.

In the following experiments mostly the right-hand side doublets are used for analysing (see Figure 14). Meaning that under the main focus are four adenosine doublets and one nicotinamide doublet.

5.2.1 Relaxation dependance on temperature and magnetic field

For this part of the work, ^1H and nh-PHIP measurements were conducted to determine the effect of temperature and magnetic field on T_1 and T_2 relaxation time constants. Firstly, temperature measurements were performed to prepare for subsequent relaxation experiments at different field strengths.

5.2.1.1 Optimal temperature for hyperpolarisation experiments

The behavior of chemical substances varies with different temperatures. This variability encompasses properties such as the state of matter, reaction rates, molecular formation and decomposition, as well as the stability of complexes. In the spectrum, chemical compounds, including analytes, exhibit higher intensity when the environmental conditions are favorable for their presence. Therefore, different temperatures were explored to determine the most suitable conditions for the chemical compounds under investigation.

First preliminary temperature measurements were conducted at four different temperatures and samples were prepared as described in Chapter 5.1.3. In addition to a typical room temperature (25°C), three more temperatures – 5°C , 15°C and 35°C – were chosen from literature as these are the most commonly used ones in NMR nh-PHIP measurements. With every complex and analyte there exist upper temperature values above which the *parahydrogen* and analyte exchange occurs too quickly and complex stays together for too

short period of time. It means that it is impossible to detect with NMR spectroscopy. What is more, methanol's boiling point is 65°. Therefore, measuring at higher temperatures with *parahydrogen* bubbling increases evaporation and sample volume changes too much during the experiment. Hence, temperatures exceeding 35°C are not ideal due to the aforementioned reasons.

This experiment was conducted with the intention of potentially reducing the number of measurements and the overall measurement time in subsequent experiments. This is particularly relevant considering that the later T_1 and T_2 relaxation measurements are approximately ten times longer in duration. By optimising the conditions in this preliminary experiment, it is possible to streamline the subsequent experiments and achieve more efficient data acquisition.

The effectiveness of hyperpolarisation increases with temperature. For example, the integral value of the nicotinamide signal at 15°C is 4.4 times higher than at 5°C. Increasing the temperature from 15°C to 25°C results in an additional 3.1 times increase, and going from 25°C to 35°C results in an additional 1.9 times increase. At the extremes of 5°C and 35°C, the latter has a 26.5 times higher integral value, indicating a much stronger signal compared to 5°C. This is also evident in Figure 16, where the signal at higher temperatures is most intense. This means that higher temperatures are favoured for $[\text{Ir}(\text{H})_2(\text{IMes})(\text{mtz})_2\text{X}]^+$ complexes, where X refers to adenosine or nicotinamide.

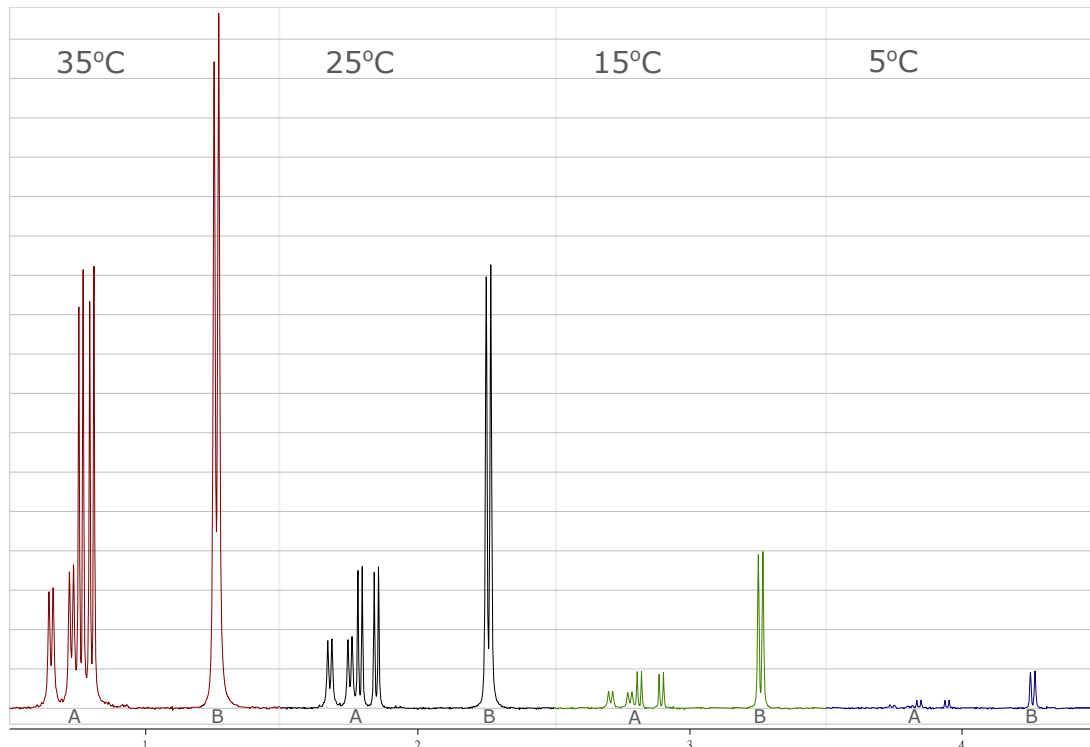


Figure 16. Influence of temperature on the effectiveness of hyperpolarisation. Four measurements are stacked from analyte signals area -22.5...-23.1 ppm. A marks adenosine signals and B nicotinamide doublet.

The chemical shift is temperature-dependent, as illustrated in Figure 17. The areas of the adenosine signals show slight shifts with lower temperatures. It is possible to observe that the nicotinamide signal chemical shifts remain unchanged, but this is only due to the fact that the spectra are aligned using that doublet. At 35°C the distance between signals decreases, leading to signal overlap and difficulties in integration. Difference in chemical shift is one reason to avoid increasing the temperature further, as it would result in more overlapping signals from the adenosine complex.

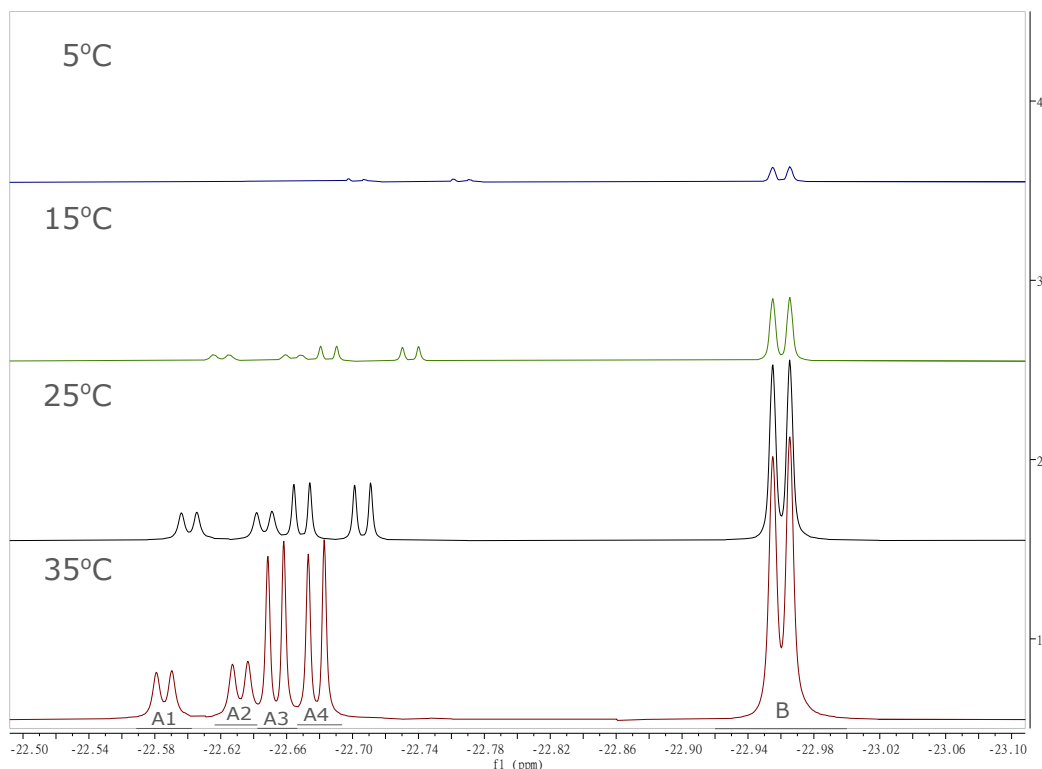


Figure 17. nh-PHIP temperature experiments with range of 5°C to 35°C with 10°C step of iridium complex, made from IMes and mtz, with adenosine and nicotinamide in -22.5 to -23.1 ppm region illustrating the temperature effect on chemical shifts. Spectra are aligned with nicotinamide signal. Areas from which T_1 and T_2 relaxation time constants were measured in following experiments are marked on the bottom spectrum. Adenosine signal areas for 35°C measurement are marked with A1, A2, A3 and A4 and nicotinamide region is B.

In contrast, measurements taken at 5°C revealed a weak signal intensity due to the iridium complex's hyperpolarisation effectiveness decreasing at lower temperatures. When temperature drops, *parahydrogen* and analyte exchange with iridium complex slows down (see Figure 11 arrows). The formation of iridium complex with the analyte and its subsequent dissociation also have an effect on the signal intensity. *Parahydrogen* needs to be refreshed continuously, because it quickly relaxes back to its equilibrium state when it comes into contact with iridium. Weighted average speed of new *parahydrogen* molecule and new analyte attaching to and detaching from the iridium complex differs when looking at different temperatures.

Parahydrogen molecule and analyte exchanges depend on the temperature, co-substrate, analytes and solvent in use. Hydrogen solubility in methanol increases with temperature. Therefore, for lower temperatures there will be less *parahydrogen* in the solution. Also the hyperpolarisation amplification is different for different analytes. For example nicotinamide signal will be amplified by thousand times ([9]) compared to the regular NMR measurement, but amino acids are amplified only 300 times. For some other analytes and/or complexes 5°C may be the best for complexation. For instance, nicotinamide demonstrates better performance at 25°C, whereas amino acids exhibit better performance at 5°C.

Taking into account the above, signal intensity at 5°C is clearly too weak for adenosine and nicotineamide (see Figure 16). In addition to that, adenosine and nicotineamide ratios with iridium symmetric complex, especially adenosine one, are also approximately three times smaller than in other cases. Meaning that results from this measurement are not sufficient to get any other convenient data from that and use it in following experiments.

Experiments at other temperatures gave out enough signal to continue in the next phase of the project – choosing the optimal temperature for relaxation experiments. What is more, T_1 and T_2 relaxation time constants may not be in correlation with signal intensities. Therefore, the relaxation experiments will be done at 15°C, 25°C and 35°C.

5.2.1.2 Temperature influence on T_1 and T_2 relaxation on 800 MHz spectrometer

For this part chemist synthesized deuterated versions of IMes and mtz (Figure 18), respectively referred $[\text{Ir}(\text{Cl})(\text{COD})(\text{IMes-d}_{22})]$ and mtz-d_5 henceforward. 22 out of 24 hydrogens in IMes are deuterated. Remaining two positions are not deuterated as they are far away from analyte complexation site. Additionally, Rayner *et al.* [32] has shown $[\text{Ir}(\text{Cl})(\text{COD})(\text{IMes-d}_{22})]$ efficiency over $[\text{Ir}(\text{Cl})(\text{COD})(\text{IMes-d}_{24})]$.

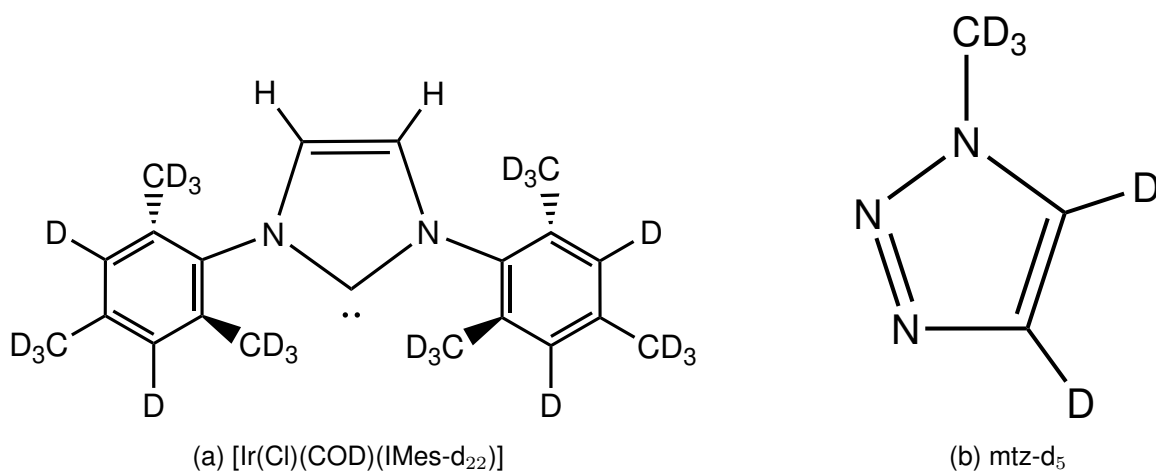


Figure 18. Deuterated compounds for active iridium catalyst.

After the formation of the active catalyst, CD₃OD was added for chemical background measurements. See Chapter 5.1.3 for more detailed samples preparation. These were performed to determine the signals originating from the co-substrate iridium complex, identify any signals indicating impurities, and detect any new cross-contamination (see Figure 19). This allowed the identification of the signals belonging to the analytes and the presence of any overlapping signals. All the signals of maroon spectrum are chemical and impurity background.

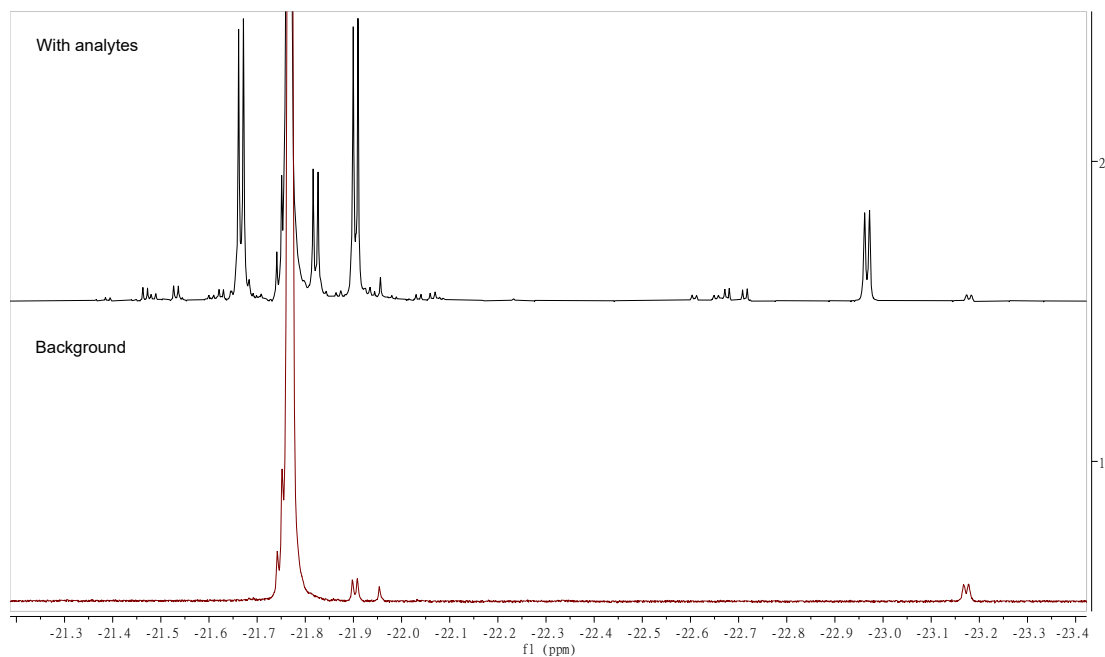


Figure 19. ¹H-NMR background spectrum of [Ir(H)₂(IMes)(mtz-d₅)₃]⁺ (maroon) and same sample with analytes (black).

From IMes, mtz and their deuterated versions four different combinations of iridium complexes were made. In Figure 20, the spectra of [Ir(H)₂(IMes)(mtz)₂X]⁺ and [Ir(H)₂(IMes-d₂₂)(mtz-d₅)₂X]⁺ are compared. X denotes adenosine or nicotinamide as the complexed analyte (this notation is used consistently throughout). ¹H-NMR spectrum of [Ir(H)₂(IMes-d₂₂)(mtz-d₅)₂X]⁺ signals are more intense than other three complexes that are in the similar intensity level.

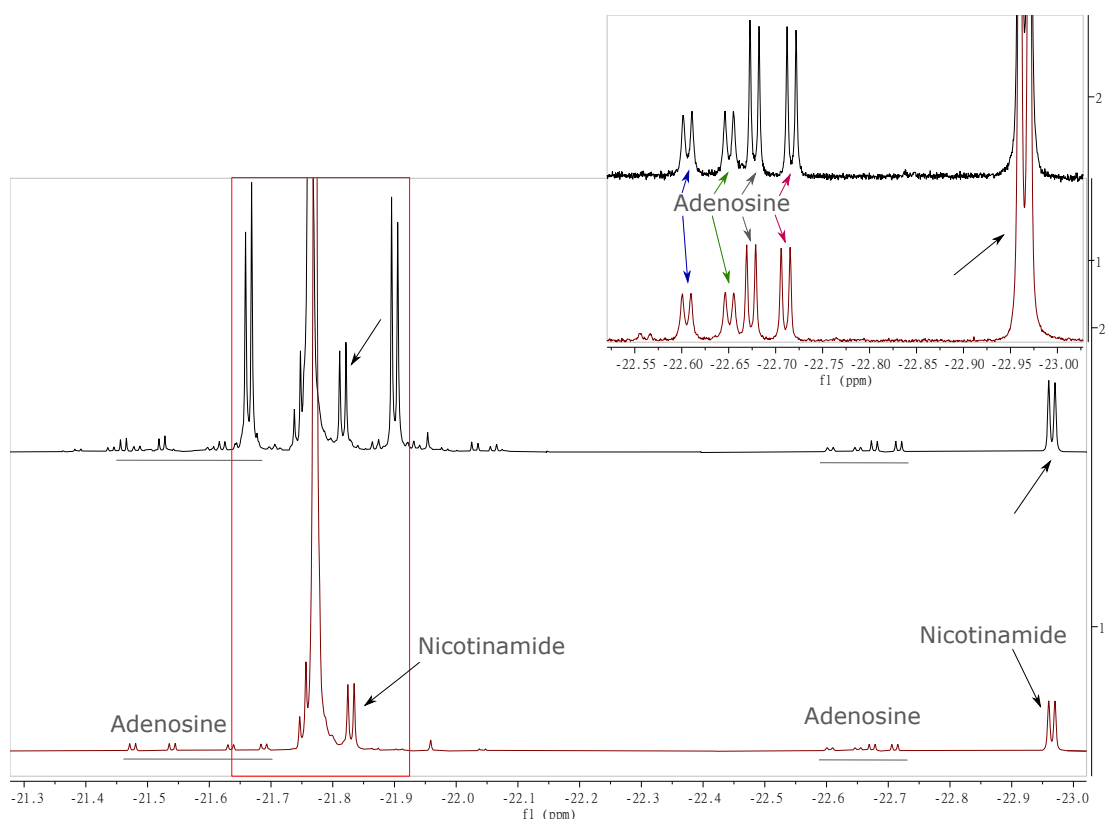


Figure 20. ${}^1\text{H}$ -PHIP measurements of $[\text{Ir}(\text{H})_2(\text{IMes-d}_{22})(\text{mtz-d}_5)_2\text{X}]^+$ (black) and $[\text{Ir}(\text{H})_2(\text{IMes})(\text{mtz})_2\text{X}]^+$ (maroon). Both measurements contain adenosine and nicotinamide as analytes.

Most striking difference is in iridium complex satellites at -21.66 and -21.90 ppm in deuterated iridium complex spectrum (see Figure 20 red box). They appear due to the deuteration of the mtz co-substrate. $[\text{Ir}(\text{H})_2(\text{IMes-d}_{22})(\text{mtz-d}_5)_2\text{X}]^+$ spectrum exhibits more signals from impurities compared to $[\text{Ir}(\text{H})_2(\text{IMes})(\text{mtz})_2\text{X}]^+$ (see Figure 20 smaller signals). As they are in small concentrations and do not overlap with analytes signals, experiments will be continued with these synthesised deuterated chemicals.

To obtain the T_1 and T_2 relaxation values, specific regions from the spectra that correspond to the right-hand side doublets of adenosine and nicotinamide were analyzed (see Figure 17). This side was chosen as this hydride is trans to analyte in iridium complex (see Figure 11).

Numbers in Appendix 1 Table 5 are T_1 relaxation time constants and Table 6 are T_2 relaxation time constants in milliseconds from those five regions, which are also marked in the bottom spectrum in Figure 17. T_2 relaxation was measured from the same samples that T_1 relaxation measurements were done. As a result, similar temperature-deuteration table was obtained (see Appendix 1 Table 6). These numbers are also shown graphically for each temperature (Figures 21, 22 and 23). As expected, T_2 values were smaller than T_1 values. The signal area for nicotinamide remained consistent in terms of chemical shift across all measurements, as it served as the reference signal for spectral alignment.

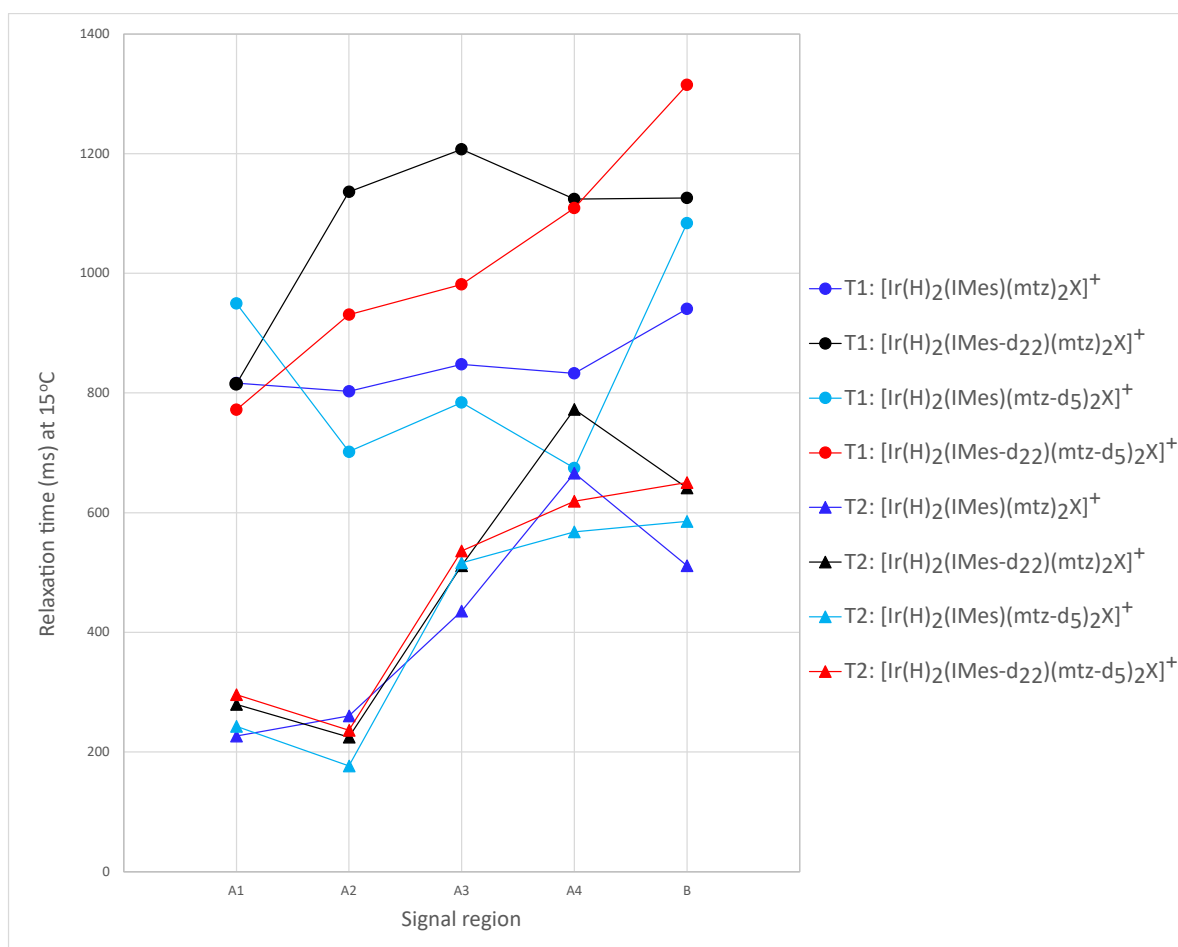


Figure 21. T_1 and T_2 relaxation time constants at 15°C for different iridium complexes. A1–A4 corresponds to adenosine and B to nicotinamide complexes signal region. Dark blue colour marks non-deuterated form, $[\text{Ir}(\text{H})_2(\text{IMes})(\text{mtz})_2\text{X}]^+$. Black colour represents data from $[\text{Ir}(\text{H})_2(\text{IMes-d}_{22})(\text{mtz})_2\text{X}]^+$. Light blue describes data from $[\text{Ir}(\text{H})_2(\text{IMes})(\text{mtz-d}_5)_2\text{X}]^+$. Red is used for deuterated form, meaning $[\text{Ir}(\text{H})_2(\text{IMes-d}_{22})(\text{mtz-d}_5)_2\text{X}]^+$. For all of these complexes, X refers to either adenosine (for datapoints A1–A4) or nicotinamide (for region B datapoints). The dots in the figure represent the relaxation time constant for T_1 , while triangles represent the relaxation time constant for T_2 .

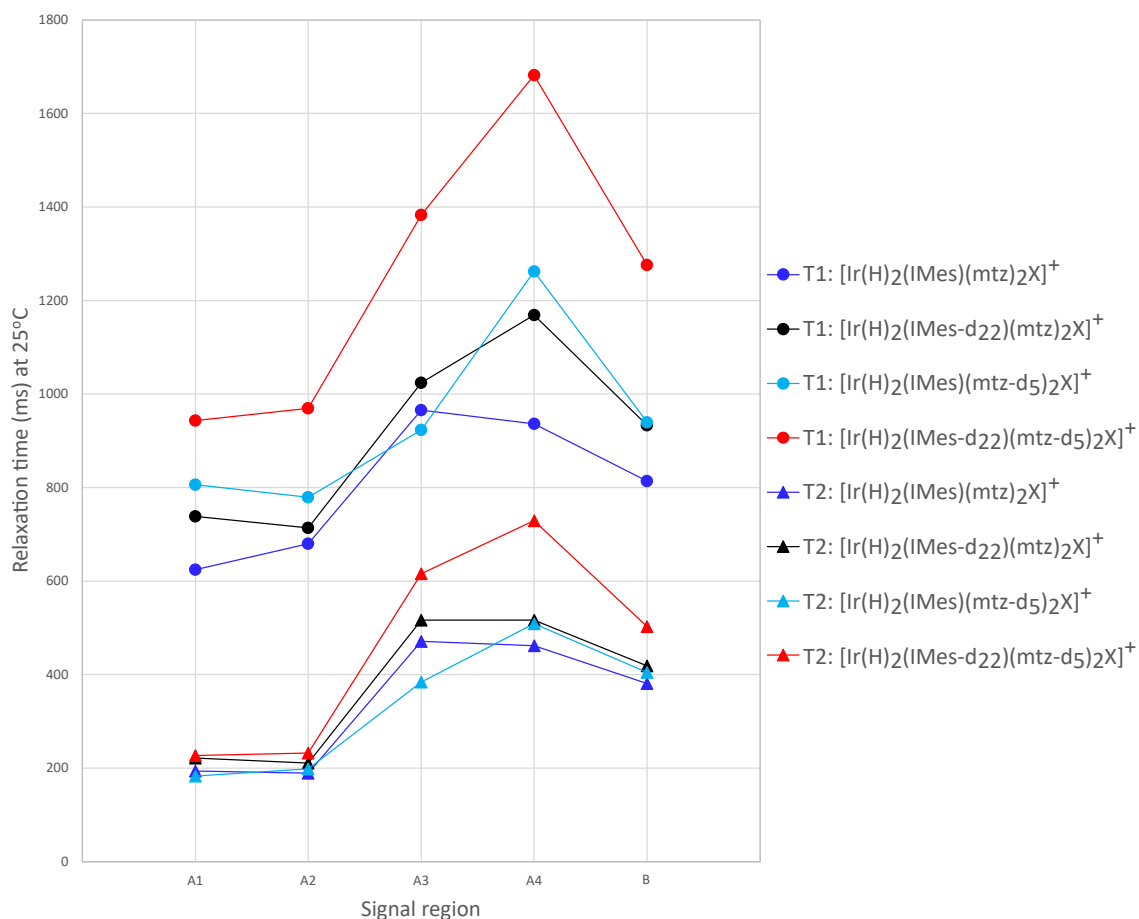


Figure 22. T_1 and T_2 relaxation time constants at 25°C for different iridium complexes. A1–A4 corresponds to adenosine and B to nicotinamide complexes signal region. Dark blue colour marks non-deuterated form, $[\text{Ir}(\text{H})_2(\text{IMes})(\text{mtz})_2\text{X}]^+$. Black colour represents data from $[\text{Ir}(\text{H})_2(\text{IMes-d}_{22})(\text{mtz})_2\text{X}]^+$. Light blue describes data from $[\text{Ir}(\text{H})_2(\text{IMes})(\text{mtz-d}_5)_2\text{X}]^+$. Red is used for deuterated form, meaning $[\text{Ir}(\text{H})_2(\text{IMes-d}_{22})(\text{mtz-d}_5)_2\text{X}]^+$. For all of these complexes, X refers to either adenosine (for datapoints A1–A4) or nicotinamide (for region B datapoints). The dots in the figure represent the relaxation time constant for T_1 , while triangles represent the relaxation time constant for T_2 .

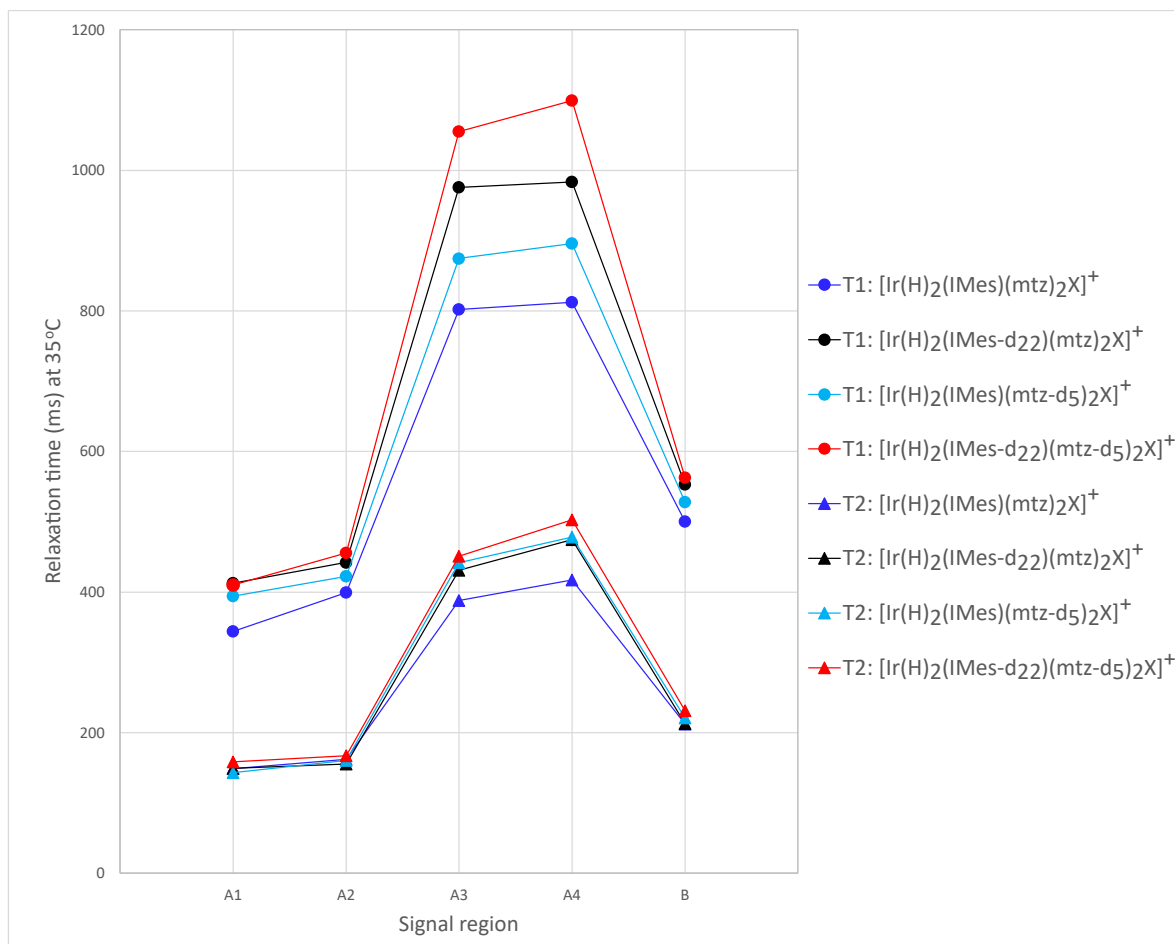


Figure 23. T_1 and T_2 relaxation time constants at 35°C for different iridium complexes. A1–A4 corresponds to adenosine and B to nicotinamide complexes signal region. Dark blue colour marks non-deuterated form, $[\text{Ir}(\text{H})_2(\text{IMes})(\text{mtz})_2\text{X}]^+$. Black colour represents data from $[\text{Ir}(\text{H})_2(\text{IMes-d}_{22})(\text{mtz})_2\text{X}]^+$. Light blue describes data from $[\text{Ir}(\text{H})_2(\text{IMes})(\text{mtz-d}_5)_2\text{X}]^+$. Red is used for deuterated form, meaning $[\text{Ir}(\text{H})_2(\text{IMes-d}_{22})(\text{mtz-d}_5)_2\text{X}]^+$. For all of these complexes, X refers to either adenosine (for datapoints A1–A4) or nicotinamide (for region B datapoints). The dots in the figure represent the relaxation time constant for T_1 , while triangles represent the relaxation time constant for T_2 .

In Figure 21, which shows the measurements taken at 15°C, the relaxation time constant for the first four data points (A1 to A4), which correspond to adenosine, varies. For the $[\text{Ir}(\text{H})_2(\text{IMes})(\text{mtz})_2\text{X}]^+$ the T_1 relaxation values are quite similar, around 800 milliseconds. Other three cases do not show as stable T_1 relaxation time constants. Especially $[\text{Ir}(\text{H})_2(\text{IMes})(\text{mtz-d}_5)_2\text{X}]^+$ complex, whose values do not follow the pattern of any other complex. However, A4 datapoint from that measurement (light blue) might be outlier as it shows a lot smaller value compared to others. In addition going on from A3 to A4, the relaxation time constant decreases whilst other complexes A4 relaxation time constant is longer than for A3. More experiments need to be done to determine if it is the outlier or is this complex specific behaviour.

At 15°C, the iridium ligand has a greater effect on the T_1 relaxation time constant of the iridium

complex with adenosine than the co-substrate. Specifically, the sample with $[\text{Ir}(\text{Cl})(\text{COD})(\text{IMes-d}_{22})]$ has a longer T_1 relaxation time constant compared to the sample with a deuterated co-substrate. However, for nicotinamide T_1 and both analytes' T_2 relaxation, $[\text{Ir}(\text{H})_2(\text{IMes-d}_{22})(\text{mtz-d}_5)_2\text{X}]^+$ shows prolonged relaxation time constants. This example provides evidence that deuteration has an effect on T_1 relaxation time constant in nh-PHIP measurements.

When examining the measurements obtained at 25°C, more similar patterns in T_1 and T_2 relaxation time constants emerge, both when analyzing them separately and when considering them together. Red, black and dark blue lines in the Figure 22 are in the same order for both relaxation values. However, $[\text{Ir}(\text{H})_2(\text{IMes})(\text{mtz-d}_5)_2\text{X}]^+$ datapoints are still jumping around other measurements, especially for A3 and A4. On the other hand, $[\text{Ir}(\text{H})_2(\text{IMes})(\text{mtz-d}_5)_2\text{X}]^+$ gap for A3 to A4 values are similar with $[\text{Ir}(\text{H})_2(\text{IMes-d}_{22})(\text{mtz-d}_5)_2\text{X}]^+$ corresponding data. For both A4 relaxes notably faster than A3. Meanwhile the signal relaxation time constants for the first diastereomer of adenosine appear to be similar within one sample.

Measurements at 35°C show even more similar relaxation time constants amongst all the complexes. Differences between chemical compounds T_1 and T_2 relaxation time constants (separately) are with rather equal differences at 35°C (see Figure 23). A correlation can be observed between A1-A2 and A3-A4: the second signal of the diastereomer relaxes slightly slower, but the values remain similar. Additionally, the complex with mtz-d₅ shows a similar pattern to the other three complexes. This means that those four complexes kinetics exchange rate window becomes smaller.

Looking all three temperatures (Figures 21, 22, 23) at the same time, overall trend is that A2 T_2 relaxation time constant raises compared to corresponding value of A1 with temperature rise. The smallest differences in T_2 relaxation time constants over all the analysed regions (A1–A4 and B) at a given temperature are observed for the non-deuterated form, i.e., $[\text{Ir}(\text{H})_2(\text{IMes})(\text{mtz})_2\text{X}]^+$. Biggest difference is in deuterated form, $[\text{Ir}(\text{H})_2(\text{IMes-d}_{22})(\text{mtz-d}_5)_2\text{X}]^+$, where the difference between lowest and highest relaxation value is 3.1 times. T_2 relaxation time constant average difference between lowest and highest relaxation value among one temperature is 2-2.5 times. This is an example that deuteration can change relative relaxation time constants within one sample.

Nicotinamide relaxation time constant change acts similarly for all of the measured temperatures as the deuteration order for T_1 or T_2 relaxation time constants stays rather same – deuterated complex, complex with deuterated ligand, complex with only deuterated co-substrate and lastly, with fastest relaxation time constants, non-deuterated complex. What is more, different complexes signal region B values get closer to each other with temperature rise. Meaning that deuterating the ligand and co-substrate lose their potential value with temperature rise.

Nicotinamide complex both relaxation time constants diminish when going to higher tem-

peratures. This is the opposite to signal intensity change (see also Figure 17). Spectrum is more intense with higher temperature. Meaning that spectral intensity and nicotinamide relaxation time constants have an inverse relationship. Therefore, depending on the wanted end result, more intense spectrum may not be always the best option as chemical compound may relax too quickly for needed measurement. This is important note, as if the experiment series would have continued with only 35°C measurements, leaving 15°C and 25°C out, this finding would have been missed.

Three complexes with at least one part deuterated demonstrate that deuteration does not have to prolong all the relaxation values compared with non-deuterated form, but in most cases will (see Figures 21, 22 and 23 dark blue line compared to others). Furthermore, deuterated part of the complex plays also a role. It has bigger impact at 15°C compared to 25°C and 35°C. This applies for both, T_1 and T_2 relaxation time constants. For example, when looking at 15°C and 25°C T_1 relaxation time constant changes. In the $[\text{Ir}(\text{H})_2(\text{IMes})(\text{mtz-d}_5)_2\text{X}]^+$ case, the T_1 relaxation time constants of A1, A2, and B regions diminish, while the T_1 relaxation time constants of the A3 and A4 regions increase. This suggests that the diastereomers have different behavior with respect to T_1 relaxation time constant.

Nevertheless, some interesting relations will come out. There are some correlations in the way relaxation time constants increase or decrease. However, there are outliers in A1 and A2 regions that do not follow universal decreasing/increasing rule. In other words, sometimes from going A1 to A2, relaxation time constant of one complex decreases and another one increases, but it is not constantly with same complexes. For example, see Figure 21 A1 and A2 different complexes relaxation behaviour. Therefore, the correlation must be studied more before further conclusions will be made. Until then it can be said that there is some correlation but strength of it will remain undetermined.

When examining Table 6 in its entirety (see Appendix 1), one can identify the optimal case for T_2 relaxation time constant. The deuterated form of the iridium complex shows the largest difference compared to the non-deuterated complex, particularly at a temperature of 25°C. Same can be said for T_1 relaxation time constant where the change in value is even bigger (see Table 5 in Appendix 1).

Deuterated and non-deuterated complex T_1 and T_2 ratios are shown in Table 3. They are obtained by dividing deuterated sample relaxation time constant with non-deuterated sample corresponding value. Deuteration effectiveness for the first two adenosine doublets is quite low for T_2 relaxation. Other adenosine and nicotinamide doublets show better relationship, especially A4. However, T_1 relaxation has noteworthy growth in values. With 50% longer relaxation time constant longer radio frequency pulses can be used and by that additional information of the sample collected.

Table 3. Relaxation time constant ratios between $[\text{Ir}(\text{H})_2(\text{IMes-d}_{22})(\text{mtz-d}_5)_2\text{X}]^+$ and $[\text{Ir}(\text{H})_2(\text{IMes})(\text{mtz})_2\text{X}]^+$, where X = adenosine or nicotinamide, at 25°C.

Region	Relaxation time constant ratio	
	T_1 relaxation	T_2 relaxation
A1	1.51	1.17
A2	1.43	1.23
A3	1.43	1.31
A4	1.80	1.58
B	1.57	1.32

The ratios of the deuteration effect between these iridium complexes show a potential positive effect on both T_1 and T_2 relaxation. Adenosine doublet with the smallest chemical shift seems to be most temperature and deuteration dependent, as evidenced by the largest changes in both chemical shift and relaxation values during the initial temperature measurements and the temperature optimisation process. This shows that different analytes may act differently with the same complex.

By combining all aspects, including the separate effects of temperature and deuteration, as well as the temperature-deuteration relation, it is possible to deduce parameters to guide the next steps of the analysis for T_1 and T_2 relaxation. The 25°C is the optimum for adenosine and nicotinamide doublets. When considering each doublet separately, this may not be the best scenario for all of the doublets, but on average it is the best. In deuteration aspect, both extremes of deuterations, meaning $[\text{Ir}(\text{H})_2(\text{IMes})(\text{mtz})_2\text{X}]^+$ and $[\text{Ir}(\text{H})_2(\text{IMes-d}_{22})(\text{mtz-d}_5)_2\text{X}]^+$, had the highest differation in T_1 relaxation while complexed with adenosine at 25°C. Therefore, these are the iridium complexes with which the experiments will continue in the further research.

5.2.1.3 T_1 and T_2 relaxation in different magnetic fields

T_1 and T_2 relaxation time constant experiments were done in three different magnetic field strengths – 200, 400 and 800 MHz or respectively, 4.7, 9.4 and 18.8 T – in order to determine if the field has an effect on the relaxation. Secondly, to understand how much the deuteration effects are depending on the magnetic field strength. Experiments were conducted using the previously determined parameters – $[\text{Ir}(\text{H})_2(\text{IMes})(\text{mtz})_2\text{X}]^+$ and $[\text{Ir}(\text{H})_2(\text{IMes-d}_{22})(\text{mtz-d}_5)_2\text{X}]^+$ complexes at 25°C temperature. Samples were prepared as described in Chapter 5.1.3.

Spectra from measurements on the 200, 400 and 800 MHz spectrometers are stacked in Figure 24. Frequency scale is referenced with nicotinamide right hand signal left peak as in previous spectra processing. Also intensities are normalized according to the same signal. Chemical shifts are observed in most of the peaks when comparing the spectra obtained at different magnetic field strengths, which is not surprising. 800 MHz spectromter gives higher

resolution, as is evident by baseline separation of all signals (see Figure 24). At lower fields these signals will increasingly overlap.

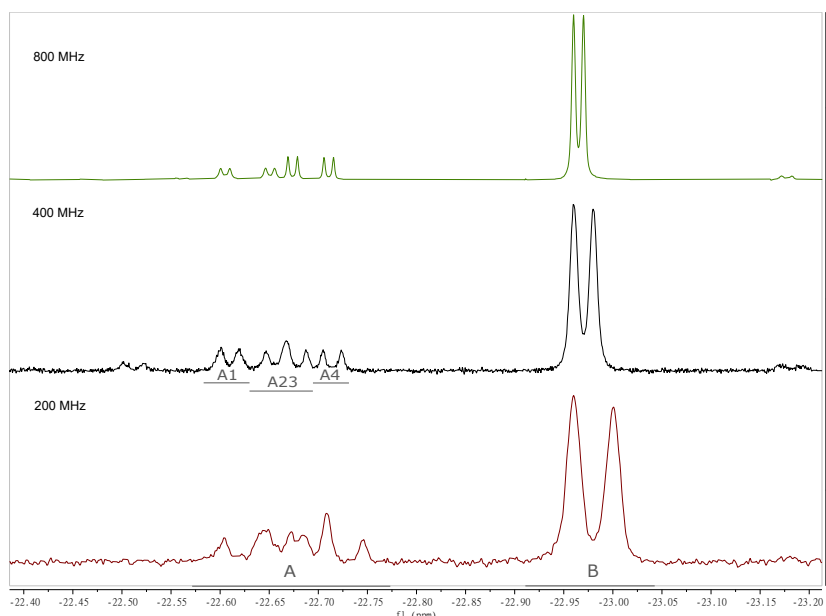


Figure 24. 200, 400 and 800 MHz spectrometers nh-PHIP spectra in comparison from -22.4 to -23.2 ppm. A1, A23, A4, and B are the signal regions for which relaxation time constants were calculated for the purpose of comparing the results obtained from 400 and 800 MHz. A and B are signal regions for which relaxation time constants were calculated for overall comparison.

Signal-to-noise ratio is better for higher field. In lower fields both of the adenosine binding sites with iridium complex seem to be equally favoured as they are with the same intensity. It can be seen better in 400 MHz spectrum as signal-to-noise ratio has higher value. In 800 MHz measurement one site might be preferred in two times out of three, because the intensity of one diastereomer pair is two times higher. However, the intensity difference might also come from the relaxation difference of those diastereomers which depends on the field strength.

Looking at the analytes complexes in Figure 24, adenosine middle doublets have overlapped in 400 MHz spectrum. Therefore, it is impossible to take separate areas for them and get T_1 and T_2 relaxation values as in previous chapter 5.2.1.2. It means that relaxation time constants are taken separately from the first and fourth doublets of adenosine, as well as from the nicotinamide doublet. For the overlapping second and third doublets of adenosine, the relaxation time constants are taken together. It creates four relaxations regions instead of the five that were previously observed. Same four regions are taken from measurements done previously with 800 MHz spectrometer for the data comparability (see figures 25 and 26 Table 7 in the Appendix 1).

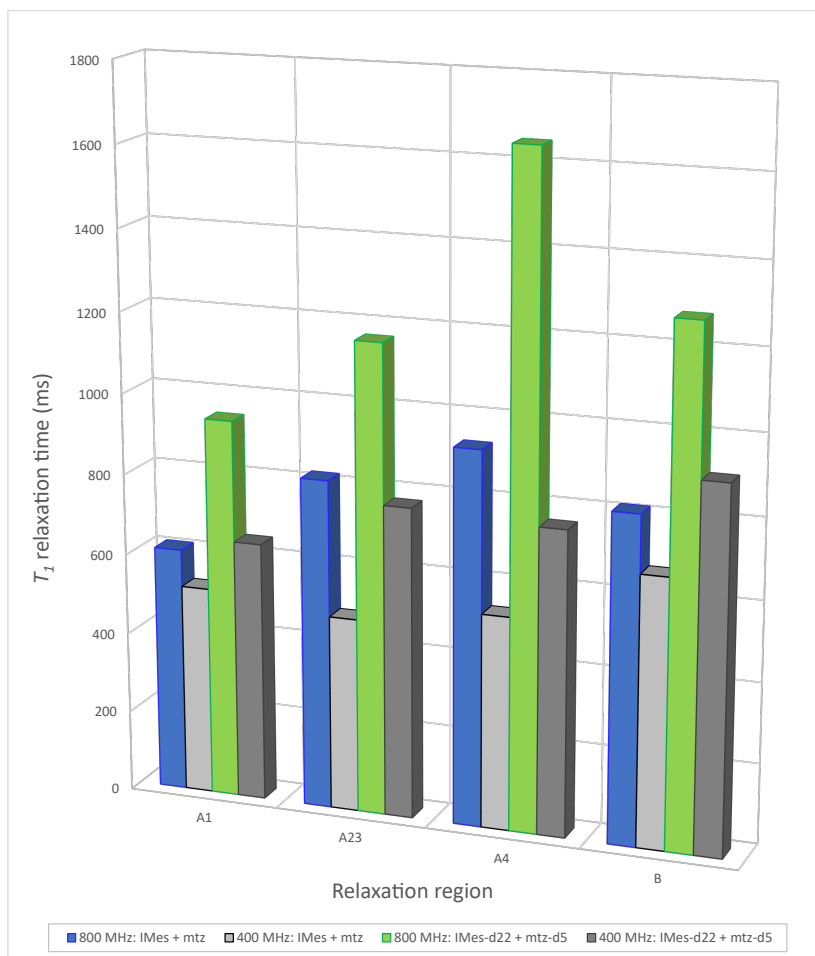


Figure 25. T_1 relaxation time constants for 800 and 400 MHz spectrometer measurements of adenosine complex signal regions A1, A23, A4 and nicotinamide signal region B (shown in Figure 24 black spectrum). Both complex's – non-deuterated and deuterated – relaxation time constants are presented.

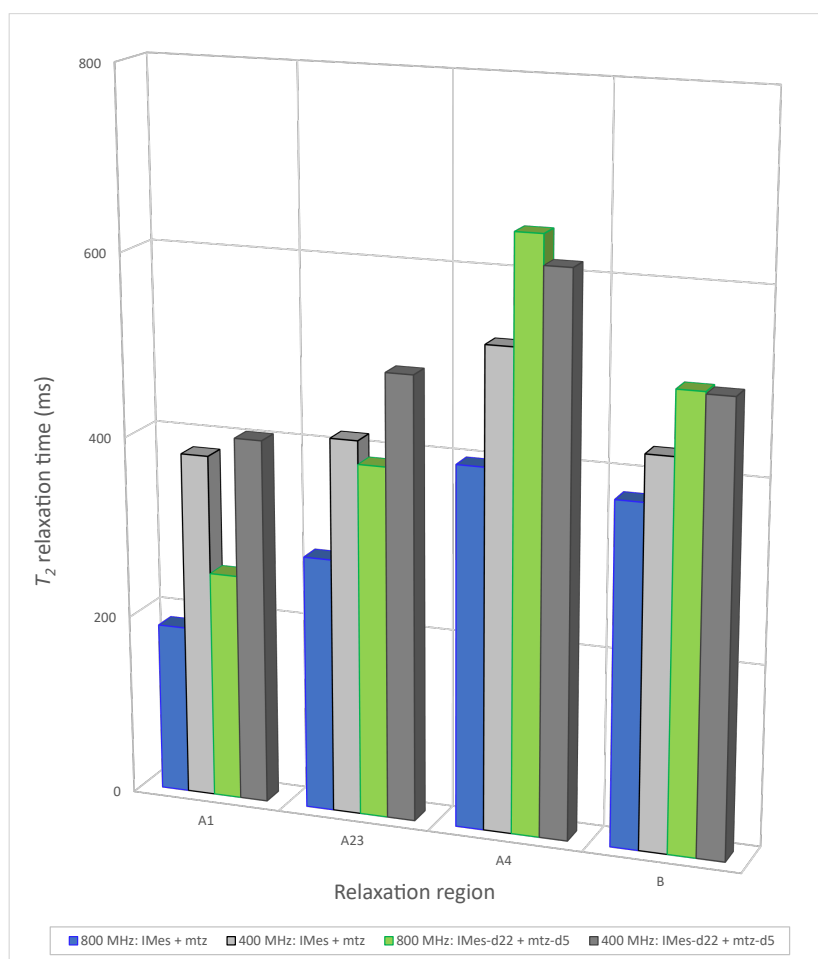


Figure 26. T_2 relaxation time constants for 800 and 400 MHz spectrometer measurements of regions (shown in Figure 24 black spectrum). Both complex's – non-deuterated and deuterated – relaxation time constants are presented.

T_1 relaxation time constants are smaller in lower field and deuteration has slightly smaller effect on most of the areas. Only exception is A23 doublet, which contains signals from adenosine second and third doublet. A23 T_1 relaxation value increases more in $[\text{Ir}(\text{H})_2(\text{IMes-d}_{22})(\text{mtz-d}_5)_2\text{Ade}]^+$ case compared to the $[\text{Ir}(\text{H})_2(\text{IMes})(\text{mtz})_2\text{Ade}]^+$.

Opposed to T_1 relaxation, T_2 values are notably higher for lower field in all regions. The use of the deuterated form does not result in a significant increase in relaxation time constant beyond what is already observed at 400 MHz field. Gain with $[\text{Ir}(\text{H})_2(\text{IMes-d}_{22})(\text{mtz-d}_5)_2\text{X}]^+$ is less than 20%. However, $[\text{Ir}(\text{H})_2(\text{IMes})(\text{mtz})_2\text{X}]^+$ already gives longer T_2 relaxation in 400 MHz magnetic field than 800 MHz with $[\text{Ir}(\text{H})_2(\text{IMes-d}_{22})(\text{mtz-d}_5)_2\text{X}]^+$ for the adenosine regions A1 and A23. Other two regions give lower values with the deuterated iridium complex in 400 MHz spectrometer compared to the 800 MHz spectrometer measurement. Still, those values do not differ much.

Looking back at the 200 MHz spectrometer measurement in Figure 24 (lower spectrum), signal-to-noise ratio is rather poor. It is not possible to calculate separate T_1 and T_2 relaxation

time constants for the peaks. Therefore, only two integrals are taken: one from the adenosine area (region A) and one from the nicotinamide doublet (region B), as shown in Figure 24. Same relaxation calculation is done with 400 and 800 MHz spectra for data comparability (see Figure 27 and 28 and table 8 in the Appendix 1).

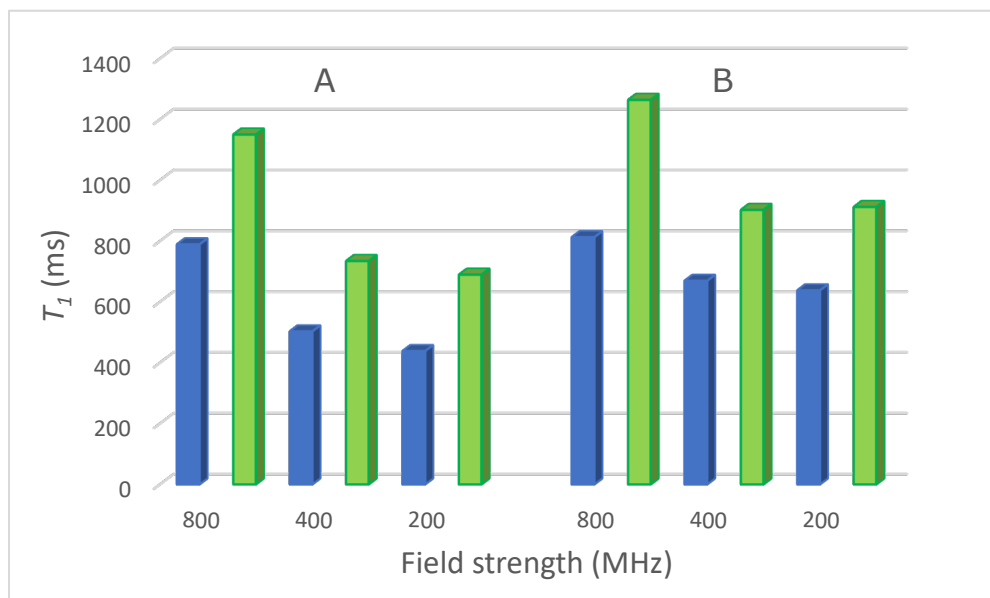


Figure 27. T_1 relaxation time constants for 800, 400 and 200 MHz spectrometer measurements. Blue represents $[\text{Ir}(\text{H})_2(\text{IMes})(\text{mtz})_2\text{X}]^+$ and green $[\text{Ir}(\text{H})_2(\text{IMes-d}_{22})(\text{mtz-d}_5)_2\text{X}]^+$, where X refers to adenosine or nicotinamide. Region A is for adenosine complex and B nicotinamide complex.

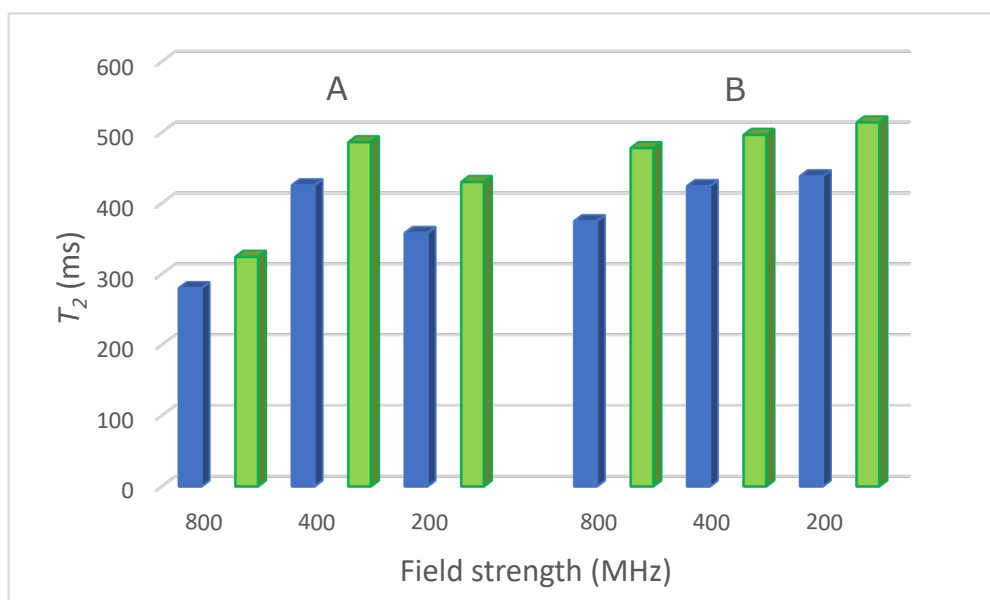


Figure 28. T_2 relaxation time constants for 800, 400 and 200 MHz spectrometer measurements. Blue represents $[\text{Ir}(\text{H})_2(\text{IMes})(\text{mtz})_2\text{X}]^+$ and green $[\text{Ir}(\text{H})_2(\text{IMes-d}_{22})(\text{mtz-d}_5)_2\text{X}]^+$, where X refers to adenosine or nicotinamide. Region A is for adenosine complex and B nicotinamide complex.

Non-deuterated compound T_1 relaxation time constant decreases when going to lower fields. Same can be said with adenosine relaxation when complexed with deuterated compound. Regardless, nicotinamide does not follow that rule completely. Its relaxation is longer in 800 MHz field, especially for deuterated iridium complex, but comparing 400 MHz and 200 MHz it is rather similar. However, T_2 do not act similarly. In 800 MHz field T_2 values are lowest for both regions. Adenosine and nicotinamide areas relax with similar times in 400 MHz spectrometer. Nevertheless, going on to 200 MHz field, adenosine relaxes faster and nicotinamide slightly slower compared to the 400 MHz field.

These measurements from the 400 MHz spectrometer can be explained by correlation and relaxation time constant plots. Longer correlation times are associated with higher fields. The experimental data are conceptually visualised in the Figure 29.

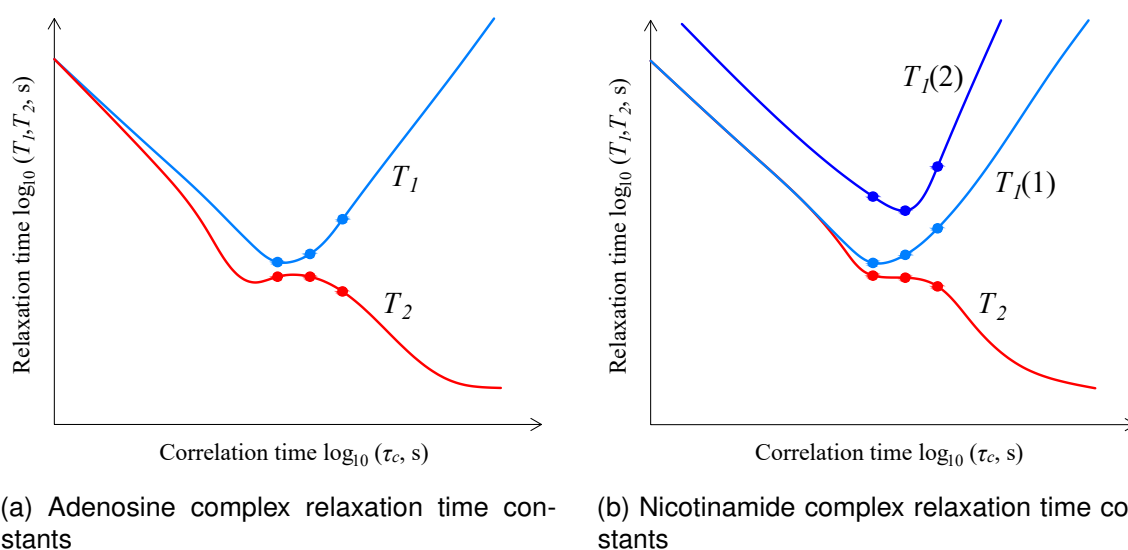


Figure 29. Conceptual illustrations of T_1 and T_2 relaxation time constants for adenosine and nicotinamide complexes. From left to right dots on the lines represent values from 200, 400 and 800 MHz spectrometer corresponding complexes. For adenosine signals schematics is the same for $[\text{Ir}(\text{H})_2(\text{IMes})(\text{mtz})_2\text{Ade}]^+$ and $[\text{Ir}(\text{H})_2(\text{IMes-d}_{22})(\text{mtz-d}_5)_2\text{Ade}]^+$ complexes. Same can be said for nicotinamide T_2 relaxation time constant. However, T_1 relaxation time constant behaves slightly different for $[\text{Ir}(\text{H})_2(\text{IMes-d}_{22})(\text{mtz-d}_5)_2\text{NA}]^+$ (dark blue line, marked with $T_1(2)$). $[\text{Ir}(\text{H})_2(\text{IMes})(\text{mtz})_2\text{NA}]^+$ T_1 relaxation time constant (light blue line, marked with $T_1(1)$) follows similar pattern as adenosine complexes. Correlation time is represented on the x-axis, while the relaxation time constant is represented on the y-axis.

Nicotinamide correlation time for T_1 relaxation should be around Larmor frequency as 200 and 400 MHz T_1 relaxation time constant measurements show almost plateau – values are similar, but for $[\text{Ir}(\text{H})_2(\text{IMes})(\text{mtz})_2\text{NA}]^+$ complex is a little bit faster and $[\text{Ir}(\text{H})_2(\text{IMes-d}_{22})(\text{mtz-d}_5)_2\text{NA}]^+$ slightly slower in 200 MHz measurement.

However, T_2 draws similar shapes for deuterated and non-deuterated complexes. The data points for the deuterated complex consistently fall within the plateau region, whereas the

$[\text{Ir}(\text{H})_2(\text{IMes})(\text{mtz})_2\text{NA}]^+$ complex values begin to exceed the boundary of the plateau. This is typical behaviour of middle sized molecules (see Chapter 1.2).

Figure 29 illustrates that the relaxation versus correlation time profiles for $[\text{Ir}(\text{H})_2(\text{IMes})(\text{mtz})_2\text{Ade}]^+$ and $[\text{Ir}(\text{H})_2(\text{IMes-d}_{22})(\text{mtz-d}_5)_2\text{Ade}]^+$ are similar. On the T_1 relaxation parabola, the data points are located on the right arc of the parabola. T_2 line for adenosine complexes in the figure is positioned somewhat differently. In addition to a horizontal shift, it exhibits slight differences in shape compared to the line for nicotinamide. Reason for that might be in the change of molecular kinetics. Hence, resulting in longer T_2 relaxation time constants for 400 MHz spectrometer measurements.

Relaxation value ratios, obtained previously by dividing the relaxation time constant of the deuterated sample by the corresponding value of the non-deuterated sample, are shown in the Table 4. T_1 relaxation shows averagely 47% longer relaxation with deuterated compound. However, for T_2 relaxation increase is on average only 19%. It means that deuteration has more influence on prolonging T_1 relaxation time constant than T_2 .

Table 4. Relaxation time constant ratios between $[\text{Ir}(\text{H})_2(\text{IMes-d}_{22})(\text{mtz-d}_5)_2\text{X}]^+$ and $[\text{Ir}(\text{H})_2(\text{IMes})(\text{mtz})_2\text{X}]^+$, where X refers to adenosine or nicotinamide, at 25°C in 200, 400 and 800 MHz field.

Field strength (MHz)	Region	Relaxation value ratio	
		T_1 relaxation	T_2 relaxation
800	A	1.46	1.16
	B	1.56	1.28
400	A	1.46	1.14
	B	1.35	1.17
200	A	1.57	1.20
	B	1.43	1.17

5.2.1.4 Summary

The experiments have led to the conclusion that relaxation is influenced by temperature, magnetic field strength, and the association-dissociation of the analyte with the iridium complex. Additionally, ^2H -labelling of IMes and mtz increases the hydride signals when they are both present, meaning that signals from $[\text{Ir}(\text{H})_2(\text{IMes-d}_{22})(\text{mtz-d}_5)_2\text{X}]^+$ complex are with higher intensity compared to other complexes.

Measurements showed that deuteration increases in T_1 and T_2 relaxation time constants. Although the increase is not significantly better compared to the non-deuterated form of iridium complex. Setting side by side the cost of making the deuterated catalyst precursor and co-substrate and their non-deuterated forms, the so called usual form is cheaper to make. Taking into account both the extended relaxation time constant and the cost difference, it can

be concluded that the benefits of deuteration are not as noteworthy as initially expected.

To achieve a more significant relaxation difference, new measurements should be done at lower temperatures. This is based on the findings and literature which suggests that relaxation is slower at lower temperatures. However, as previously mentioned, hyperpolarisation with *parahydrogen* and iridium complex goes down in efficiency because there is slower *parahydrogen* exchange with the iridium complex. Meaning that the signal-to-noise ratio is smaller. In addition to this, the formation of iridium complex with the analyte and its subsequent detaching should be taken into consideration also. However, measurements at lower temperatures could be carried out using chemical compounds whose complexes have better efficiency at lower temperatures as well.

5.2.2 ATP, ADP, AMP and blood NMR

Regular ^1H measurements were done according to the article [29] by supervisor before author's work and they showed the same results as the article according to which they were made (see also sample preparation in Chapter 5.1.3). The whole blood extracts contained signals for ATP, ADP and AMP in region 8.4...8.7 ppm. However, nh-PHIP measurement with iridium complex did not show any of them (see Figure 30 maroon spectrum). For the reference, ATP, ADP, AMP sodium salt standard solutions were measured by supervisor. All of them had signals in *parahydrogen* hyperpolarisation 1D and 2D measurements. Meaning that ATP, ADP and AMP can form hyperpolarisable iridium complexes.

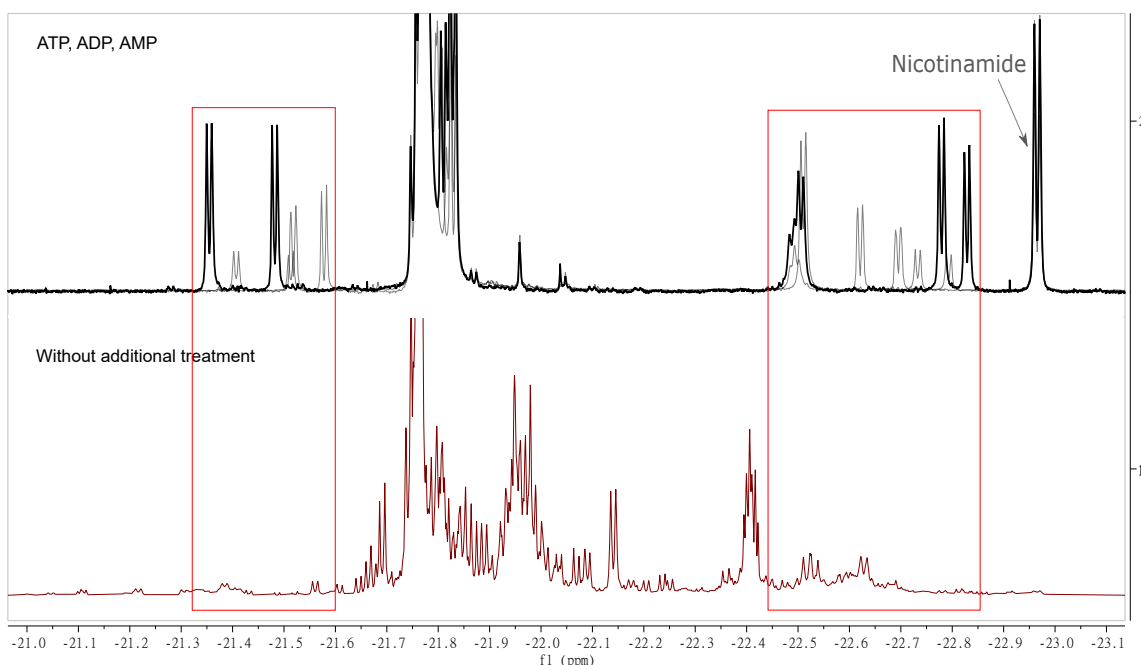


Figure 30. nh-PHIP spectrum of lyophilised whole blood extract taken up in CD_3OD (maroon). Stacked nh-PHIP spectra of ATP, ADP and AMP (black) is given for reference.

In human blood system the ATP is complexed with Mg^{2+} (see Figure 31) [21]. Moreover, the ADP is also complexed with Mg^{2+} as it is the substrate of ATP synthase (see Figure 32) [21]. Hypothesis is that this complexation with the Mg^{2+} interferes with nh-PHIP measurements so that ATP, ADP and AMP are NMR invisible or the chemical shifts are in an unknown place or the iridium complexes do not form at all. If they are NMR invisible, another hypothesis can be proposed to explain this. If any of those phosphates is complexed with magnesium, it interferes complexation with iridium complex as two positively charged ions do not want get close to each other. For that purpose, the subchapters that follow investigate the complexation with Mg^{2+} and its removal processes.

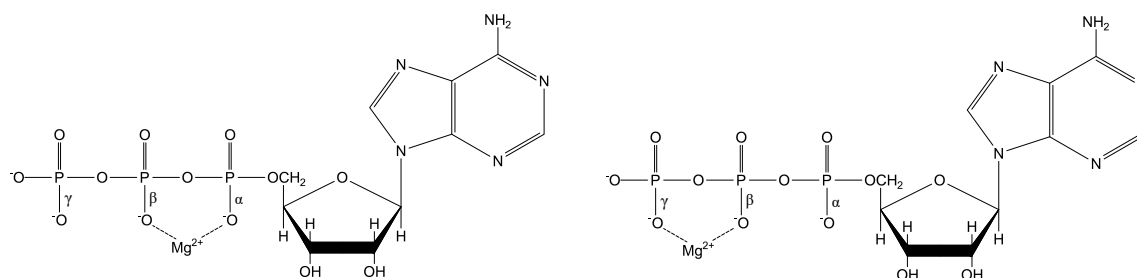


Figure 31. ATP and Mg^{2+} possible complexation sites. [33]

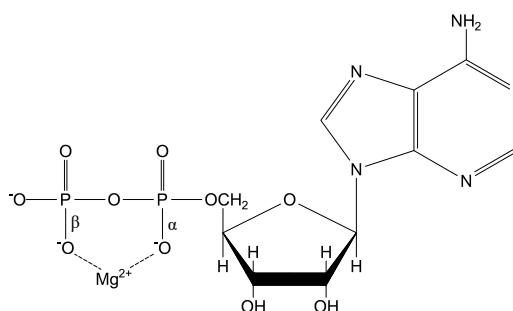


Figure 32. ADP and Mg^{2+} possible complexation site. [34]

5.2.2.1 ATP, ADP and AMP with Mg^{2+} detection

There is hypothesis that cancer's energy metabolism produces more ATP than normal cells, whereas some of the redundant ATP will leak from cancer cells into blood plasma [35, 25]. However, ATP, ADP and AMP are not seen in blood plasma with regular NMR. One possible reason for this could be that they are present at concentrations below the detection limit of regular NMR techniques. However, it might be possible to observe them using nh-PHIP. Before proceeding, it is important to determine if they complex with iridium catalyst and what are their chemical shifts. To investigate this, whole blood was initially examined since it is already known to contain the desired analytes from red blood cells at high concentrations.

Solutions with only ATP, ADP or AMP and with nicotinamide as analytes were made (see sample preparation in Chapter 5.1.3). Store bought ATP, ADP and AMP come as sodium

salts. But in human body ATP, ADP and AMP are in the form of magnesium salts. For that reason appropriate salts were prepared by using $MgCl_2$. One- and two-dimensional spectra were measured in order to bring together left- and right-hand signals. 2D spectra are shown in Figures 33, 34 and 35.

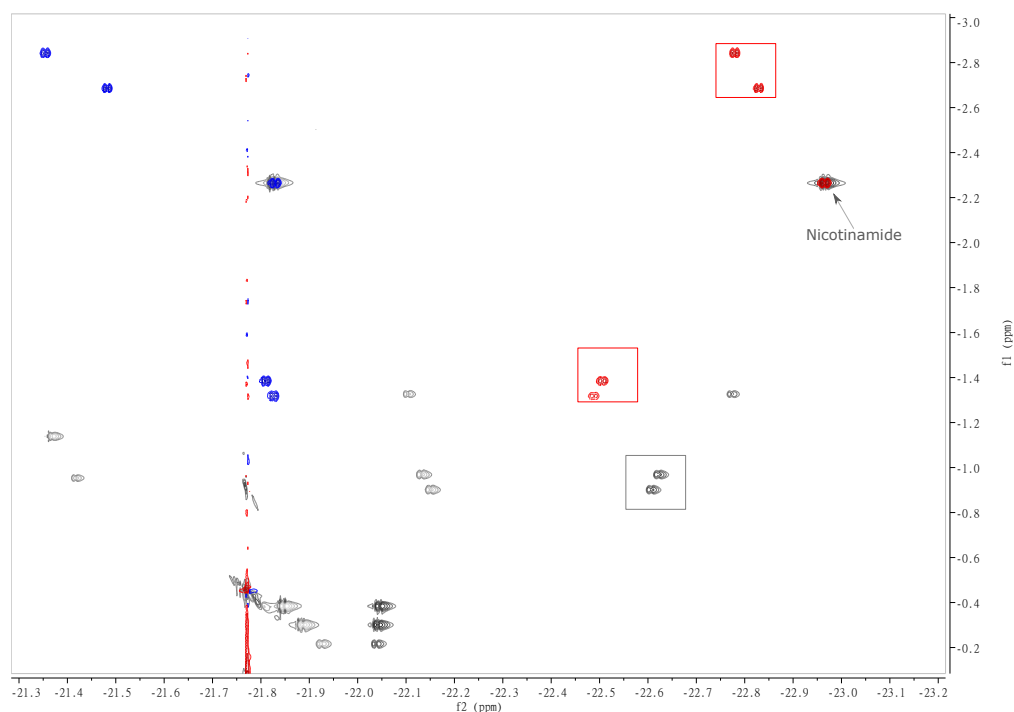


Figure 33. Overlaid ZQ-COSY spectra of ATP sodium (red-blue spectrum) and magnesium (greyscale spectrum) salts from -21.3 to -23.2 ppm in comparison. Right-hand ATP sodium hydride signals are outlined with a red box. Potential ATP magnesium signals are outlined with grey box.

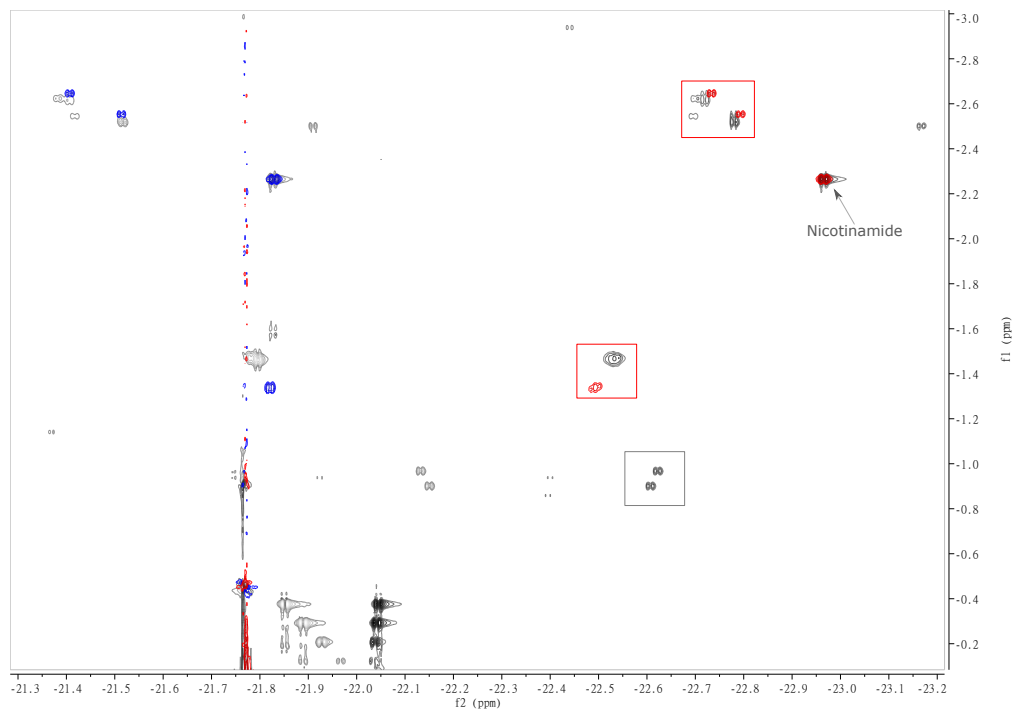


Figure 34. Overlaid ZQ-COSY spectra of ADP sodium (red-blue spectrum) and magnesium (greyscale spectrum) salts from -21.3 to -23.2 ppm in comparison. Right-hand ADP sodium hydride signals are outlined with a red box. Potential ATP magnesium signals present in Mg-ADP as cross-contamination are outlined with grey box.

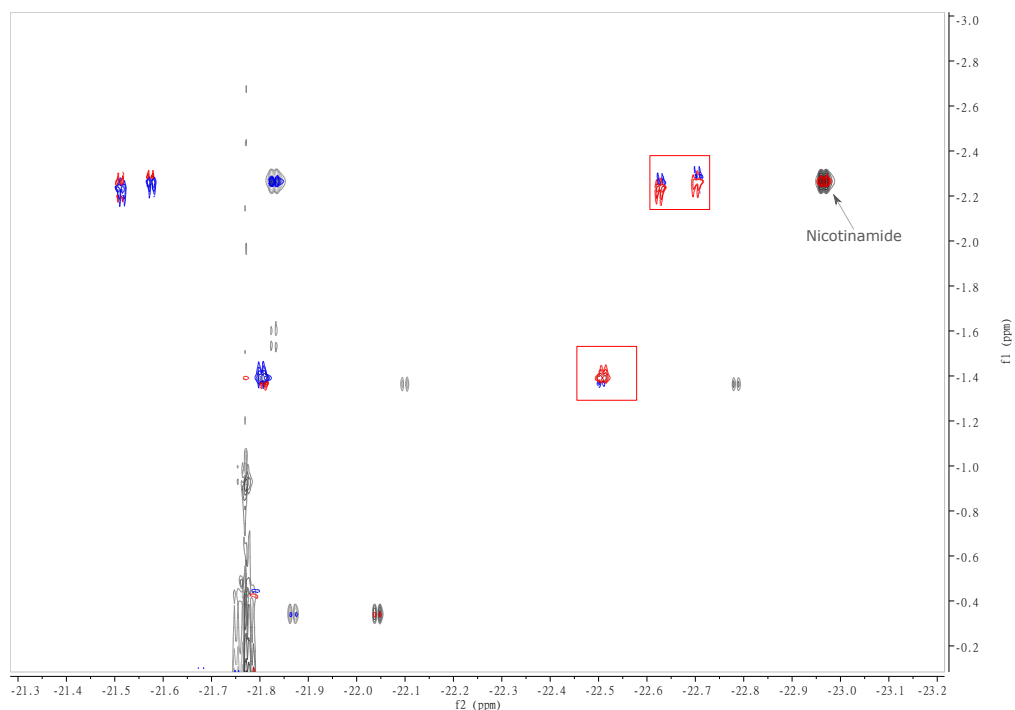


Figure 35. Overlaid ZQ-COSY spectra of AMP sodium (red-blue spectrum) and magnesium (greyscale spectrum) salts from -21.3 to -23.2 ppm in comparison. Right-hand AMP sodium hydride signals are outlined with a red box. AMP magnesium spectra did not show any new strong signals that cannot be associated with background signals.

ATP, ADP and AMP sodium salts were measured previously by supervisor. Additionally, ^{31}P spectra were measured to determine the purity of the ATP, ADP and AMP sodium salts samples. ATP contained small amount of ADP and AMP, but this could be breakdown product of ATP to ADP and AMP. ADP on the other hand contained a lot of ATP and AMP, which is probably due to cross-contamination. AMP was pure. This means that in ATP and especially in ADP some additional signals can be found.

All three analytes sodium salts complexed with iridium catalyst resulting in four hydride pairs. The two upper hydride pairs in 2D spectra (red-blue spectra in Figures 33, 34 and 35 annotated with red boxes) have more analytical value as these are more dispersed. The lower signals pairs overlap and have small chemical shift difference.

In all cases, ATP, ADP and AMP magnesium salts do not show a similar signal pattern to sodium salts (see Figures 33, 34 and 35 grayscale spectra). For Mg-AMP no signals are detected that are not from background. However, some new signals appear in the nh-PHIP measurement for Mg-ATP and Mg-ADP spectra (annotated with the grey box). These signals overlap exactly. As signals are more intense in Mg-ATP spectrum and it is known that Mg-ADP should contain also some ATP due to the cross-contamination, these signals might come from ATP magnesium salt. In spite of that, more experiments are needed to determine if these signals belong to Mg-ATP.

Additionally, Mg-ADP, signals are observed just below the ADP sodium salt signals (see Figures 34 and 36 red boxes). This shift might be caused by the pH or by the failure to form the magnesium salt. ADP sodium salt solution pH was not corrected as it was done in CD_3OD . In water ADP sodium salt pH is around 4. Mg-ADP sample's pH in water was raised from 4.08 to 8.58.

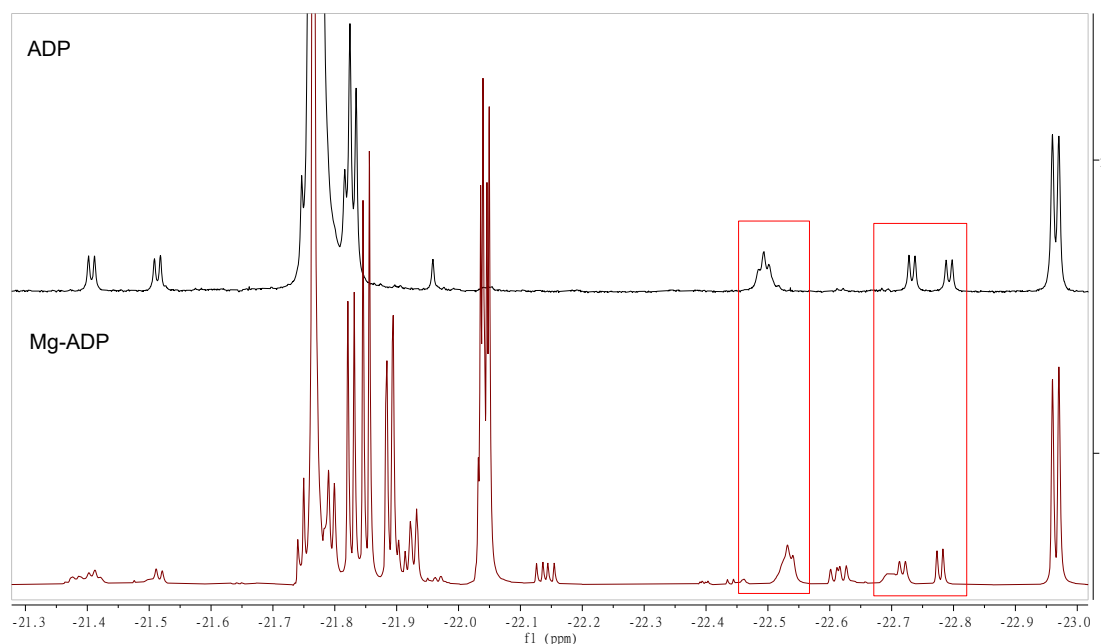


Figure 36. Mg-ADP spectrum (maroon) and ADP spectrum (black) in comparison from -21.0 to -23.4 ppm. Marked areas are the same red boxes as in Figure 34. Mg-ADP sample contains 0.3 mM ADP and 0.1 mM nicotinamide, while ADP sample has 0.1 mM ADP and 0.2 mM nicotinamide.

To sum up, solutions made with ATP, ADP and AMP magnesium salts showed that Mg^{2+} has an effect on the signals in the nh-PHIP spectra compared to sodium salts. As a magnesium salt, AMP does not show its signals. The results for ATP are inconclusive and further experiments are needed. For Mg-ADP, however, the signals are slightly shifted, but close to their expected positions, which could be due to the different pH and magnesium salt formation failure.

5.2.2.2 ATP nh-PHIP signal enhancement by 2H -labelled iridium complex

ATP detection in blood matrix is not a trivial task. ATP complex with Mg^{2+} is the reason why it is not seen in blood. This is because Mg-ATP does not form hyperpolarizable complexes with iridium.

ATP is a valuable high energy compound in the living organism and its plasma levels are usually very low. Because of this any additional signal gain is very valuable. As it was shown in previous chapter, nh-PHIP with 2H -labelled iridium complex gives even more signal enhancement. Meaning that analytes might be seen in smaller concentration. Therefore, it was looked if iridium complex deuteration nh-PHIP has similar effect with ATP as with adenosine (see also sample preparation in Chapter 5.1.3).

Deuteration of iridium complex enhances ATP signals 30–40% (see Figure 37), which is

similar to adenosine as described in previous Chapter 5.2.1. Small chemical shift can be seen for the hydride signals, especially for the left-hand side. It is expected as left-hand-side signals are from the hydride that is diagonally opposite to mtz-d₅ (see also Figure 11).

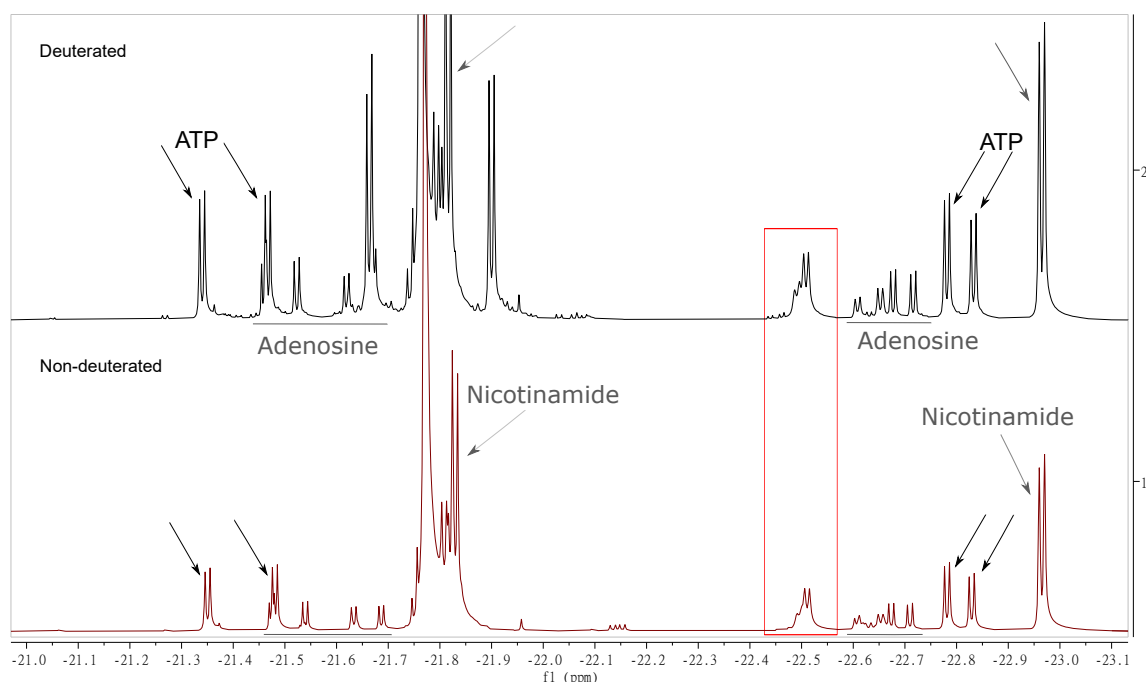


Figure 37. nh-PHIP spectrum of $[\text{Ir}(\text{H})_2(\text{IMes})(\text{mtz})_2\text{Y}]^+$ complex (maroon) compared to the $[\text{Ir}(\text{H})_2(\text{IMes-}d_{22})(\text{mtz-}d_5)_2\text{Y}]^+$ complex (black), where Y marks adenosine, nicotinamide or ATP, from -21.0 to -23.4 ppm. Samples contain 0.1 mM ATP (dissolved in CD_3OD), 0.1 mM nicotinamide and 0.07 mM adenosine. Adenosine signals are in the areas above grey line. In the red box are signals that come from ATP solution.

5.2.2.3 Two-valence-electron metal ions removal process

One of the widely used resin based compound which acts as chelating agent in binding metal ions from solution is Chelex 100 (referred as Chelex henceforward). Via binding it forms stable complexes with metal ions. [36] It is often used in the preparation of biological samples, as blood is, for analyses [37]. It should remove M^{2+} ions, which would result in more detailed NMR spectrum.

Comparing the untreated and Chelex treated whole blood extract nh-PHIP spectra, the latter is more intense and has more signals (see Figure 38 and sample preparation in Chapter 5.1.3). It can be explained by the Chelex ion removal process. Due to the complexity of 1D spectrum, 2D ZQ-COSY was done. Unfortunately, ATP, ADP and AMP signals were not detected compared to those of standard solutions. However, nicotinamide can be seen. Therefore, it can be used as the frequency axes reference point similarly as in previous work.

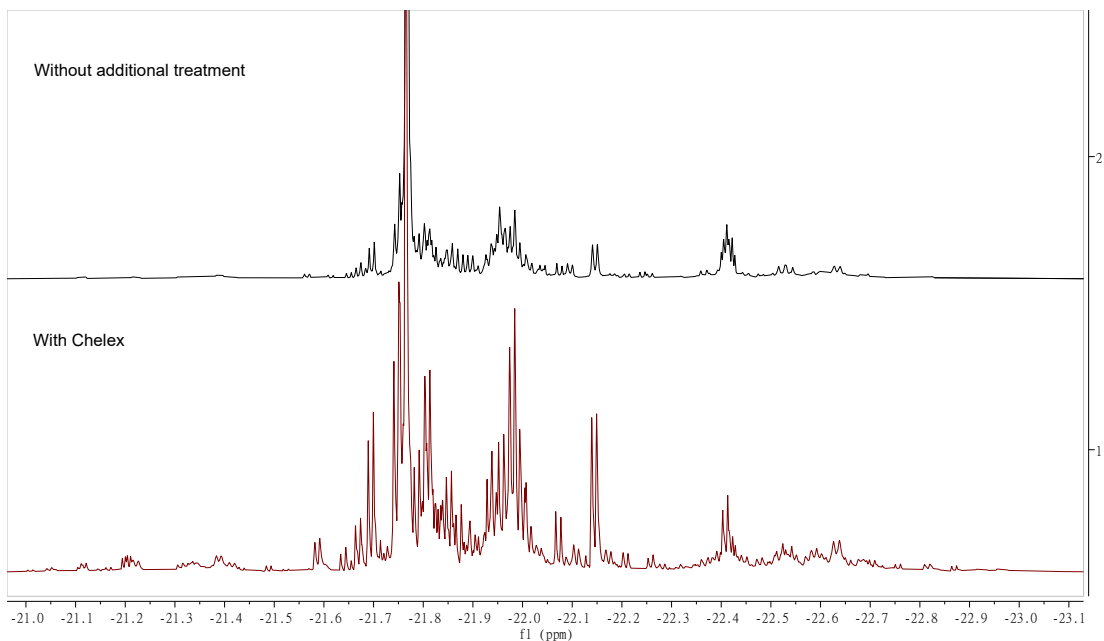


Figure 38. ^1H -PHIP spectrum of lyophilised blood taken up in CD_3OD (black) compared to the Chelex treated whole blood extract spectrum (maroon).

As the nh-PHIP measurement did not show desired analytes, normal ^1H NMR spectrum was measured from the methanolic whole blood extract. Figure 39 compares spectra of whole blood extract made with phosphate buffer (before author's contribution to this work) with Chelex treated methanolic sample. It shows that methanolic solution does not contain ATP, ADP and AMP signals. This raises hypothesis, maybe ATP, ADP and AMP are not methanol soluble.

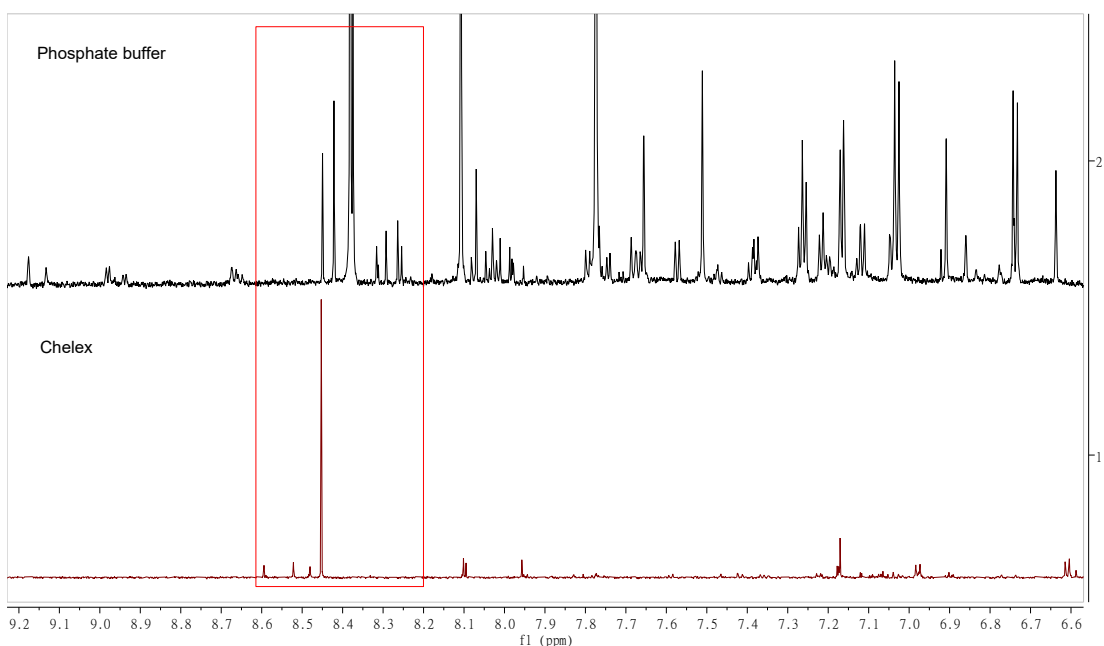


Figure 39. Comparison of ^1H spectra of whole blood extract in phosphate buffer with pH 7.5 in D_2O (black) and sample made with Chelex in CD_3OD (maroon). Area where ATP, ADP and AMP should be is marked with a red box.

Making the methanolic solution of whole blood extract, solids were centrifuged, assuming they were leftover small proteins or high-molecular weight compounds. These solids were taken up in a phosphate buffer and analysed by ^1H NMR. Phosphate buffer was made according to the article [29] and its pH was 7.51. ATP and ADP signals can be easily seen from the spectrum (Figure 40). AMP signal is also present but in smaller intensity. Therefore, the residue was not only proteins. ATP, ADP and AMP in blood do not appear to be soluble in CD_3OD .

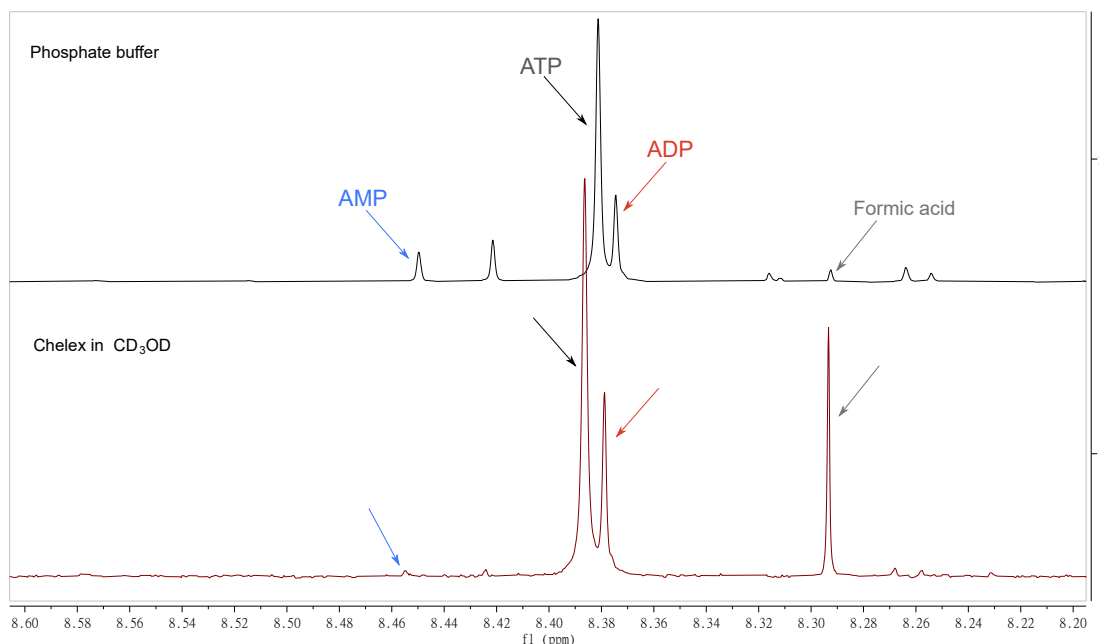


Figure 40. Comparison of ^1H spectra of whole blood extract in phosphate buffer in D_2O (pH 7.5, black) and solid residue (from Chelex treated whole blood extract taken up in CD_3OD) dissolved in phosphate buffer in D_2O (pH 7.5, maroon).

For additional confirmation ^{31}P spectrum was measured from the sample with BBO probe, which is optimised for observation of ^{31}P . For comparison, ^{31}P spectrum was measured for the whole blood extract methanolic solution. Measuring phosphorus is an additional confirmation that there is indeed no ATP in our methanol sample. In other words, from the ^{31}P spectra (Figure 41) it can be also concluded that the initial sample processing does not work, because ATP, ADP nor AMP in blood do not dissolve in CD_3OD . Their appearance in upper spectrum shows that ATP, ADP and AMP will precipitate out in methanol. Therefore, in order to see ATP, ADP and AMP lyophilised whole blood extract cannot be dissolved only in methanol.

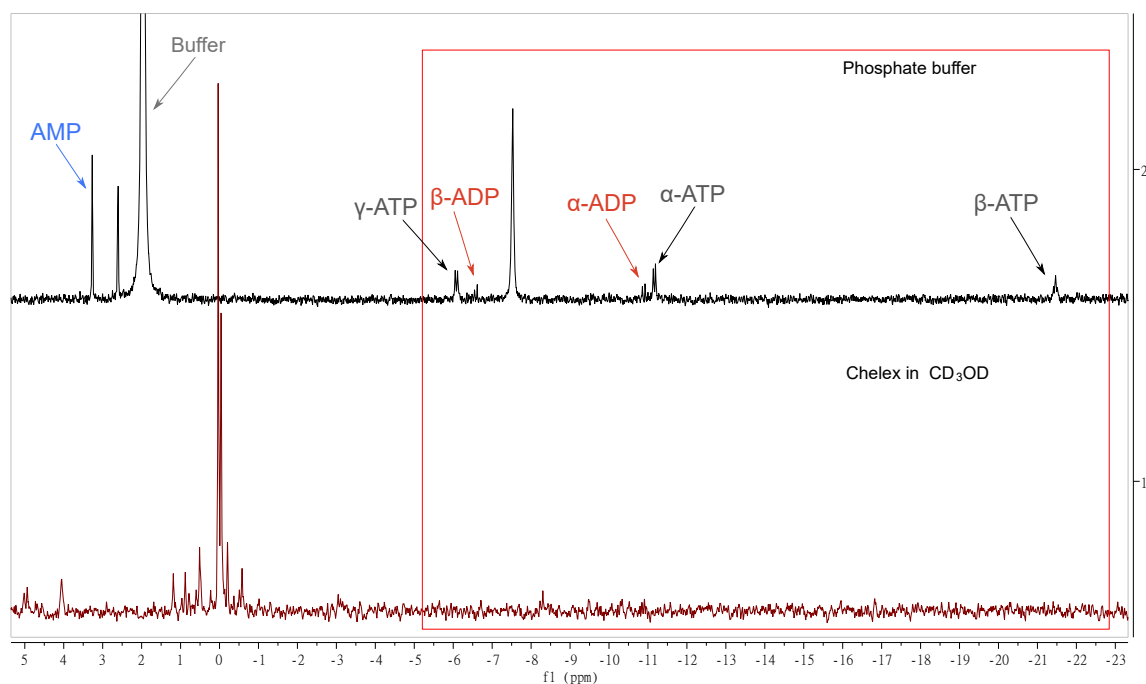


Figure 41. ^{31}P spectra of blood methanolic solution with Chelex impact (maroon) and solid residue from the same sample dissolved in phosphate buffer in D_2O (black). Red box indicates area where ATP and ADP should be. ATP and ADP signals are allocated in the upper spectrum, where they appear (see also Figure 31 and 32). AMP is the first signal from the left in the top spectrum. Broad singlet peak inside the red box belongs to the polyphosphate.

5.2.2.4 EDTA

Sample preparation with Chelex adds additional steps and takes time. It is good to use as few sample preparation steps as possible to ensure that parts of original sample are not left behind in every step. Therefore, alternatives for two-valence ions removal were considered. One possible solution to see the analyte signals, that are looked for, is using ethylenediaminetetraacetic acid (referred as EDTA) in sample preparation. EDTA is also widely used for metal ions removal.

EDTA makes it possible to work in organic solutions. In addition, it is water-soluble [38]. Blood collection tubes coated with di- (or tri-)potassium EDTA are used for most hematology procedures. EDTA acts as an anticoagulant in those tubes. It binds the calcium ions and interrupts the clotting of the whole blood extract. [39] EDTA also cleaves Mg^{2+} . Meaning that EDTA binds magnesium more strongly than ATP and exchanges it for Na^+ . Stated differently, ATP-Na is derived from Mg-ATP. Those ions are exchanged with Na^+ as EDTA disodium salt was used. Na^+ does not interfere NMR measurements. After being bound by EDTA, Mg^{2+} ions remain in solution, but are not bound to ATP, ADP or AMP [38]. Mg^{2+} complexed to EDTA does not interfere with NMR analysis any more.

Before starting working with blood extracts, it was made sure that EDTA will not complex with

iridium. To see weather EDTA has desired effect on whole blood extract, another blood extract was taken up in distilled water (see sample preparation in Chapter 5.1.3). Normal ^1H and ^{31}P spectrum were measured with BBO probe and with internal standard insert. Afterwards the EDTA solution in NaOH and distilled water were added. ^1H and ^{31}P measurements were done again.

By comparing these measurements EDTA influence is clearly seen in ^{31}P spectrum (see Figure 42). Due to that AMP, ADP and ATP have signal in the spectrum as other parameters remained the same. All of their signals are present in sample with EDTA. On the other hand, without EDTA only a minor broad signal can be seen in the marked ATP and ADP area of interest. EDTA removes magnesium ions and desired analytes appear in the ^1H spectrum (see also 43 third spectrum).

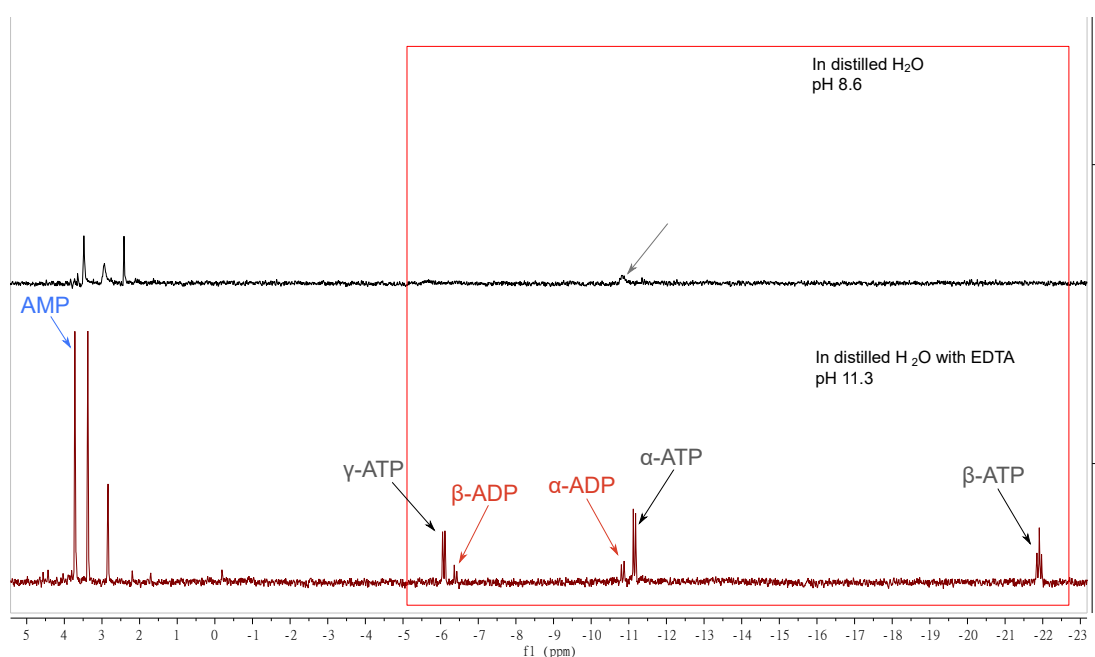


Figure 42. ^{31}P spectra of whole blood extract in distilled H_2O measured with internal standard insert (black) and same sample with EDTA in NaOH (maroon). AMP, ADP and ATP signals are identified. With EDTA ADP and ATP signals appear in the red box. Arrow in upper spectrum shows potential signal from ATP, ADP or both complexed with Mg^{2+} . AMP might have signal in upper spectrum also.

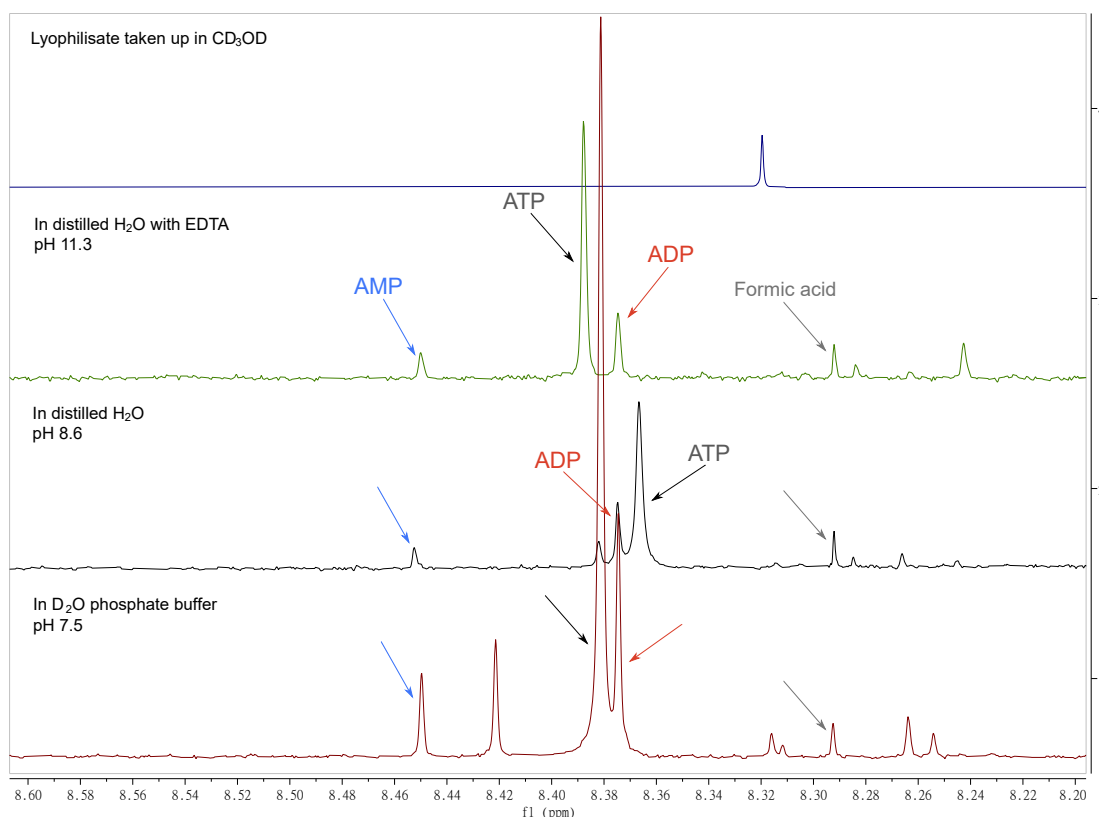


Figure 43. ^1H measurement of whole blood extract in D_2O phosphate buffer with pH 7.5 (made by supervisor, maroon). Black spectrum is a whole blood extract in distilled H_2O measured with internal standard insert with pH 8.6 and the same sample with EDTA in NaOH (green) with pH 11.3. Fourth sample (blue) contains quarter of third sample, which was lyophilised after which CD_3OD was added. pH in CD_3OD is not comparable with pH in water, therefore its pH was not measured.

By using EDTA the sample pH is influenced. Lyophilised whole blood extract taken up in water had a pH of 8.6, but by adding EDTA, pH was over 11. High pH comes from EDTA solution not from EDTA itself, because EDTA does not dissolve at lower pH. High pH value might be another obstacle as some compounds might start to decompose at such high pH values. Due to the complex nature of whole blood extract, it is not a trivial task to locate analytes. Due to the shifting of the signal's position, it becomes challenging to relocate the signal accurately as it may overlap with signals from other compounds.

Four samples from the same origin, but with different sample preparation, were analysed and compared (see Figure 43). Proton spectrum is not as drastically affected as the phosphorus spectrum by EDTA and pH change. Shifts in signals are rather from pH change than from Mg^{2+} ion removal as signal intensities grow only a little. ATP signal exhibits shifting in its position, but ADP AMP chemical shift among some other smaller peaks do not change (see Figure 43 first three spectra). pH only slightly affects the chemical shift of AMP. EDTA does not improve ATP, ADP and AMP complexed with Mg^{2+} solubility in methanol (see figures 42 and 43 upper spectra). It was previously made sure that these sample contained those analytes. Further confirming that only methanol cannot be used to dissolve the whole blood

extract. As attempts were made to do so, they remained in the solid residue. Therefore, another whole blood extract sample preparation methods were looked.

Whole blood extract from the -80°C fridge has two layers that are distinguishable with the naked eye after melting. One layer is water mixed with methanol and another chloroform layer. The water-methanol layer, should contain ATP, ADP and AMP, part of the solution was taken, CD_3OD added and ^1H spectrum measured without any other sample preparation. Unfortunately, there was considerable chloroform signal in the aromatics region overlapping with ATP, ADP signals. Even with water and chloroform presaturation analytes' signals would also be suppressed due to the proximity of the signals. In $n\text{H-PHIP}$ chloroform and water peaks do not interfere with the spectrum, because we are looking in the region far far away from their signals (around -22 ppm).

Why not to use lyophilised whole blood extract with distilled water for $n\text{H-PHIP}$ measurement if it has all the signals? Principal factor is that iridium catalyst and hydrogen are not water soluble. On top of that, it has been shown that up to 10% of water by volume can be in the *parahydrogen* measurement to obtain worthy spectrum. The maximum water volume known to be tolerated by the $n\text{H-PHIP}$ system can be 58% to get satisfactory spectrum.

As previously showed, EDTA had an effect on whole blood extract conformed with ^{31}P spectra. For hyperpolarisation measurements only water-methanol part of the whole blood extract was used with diluting in additional CD_3OD in order to minimise the water proportion in the final sample and keep it under 10%.

Four different samples were made, measured and compared to the ATP, ADP, AMP sodium salts measurements (see Figure 44). Each of those four samples contained same amount of whole blood extract water-methanol solution. EDTA amount and addition time and place varied. More detailed sample information in Chapter 5.1.3.

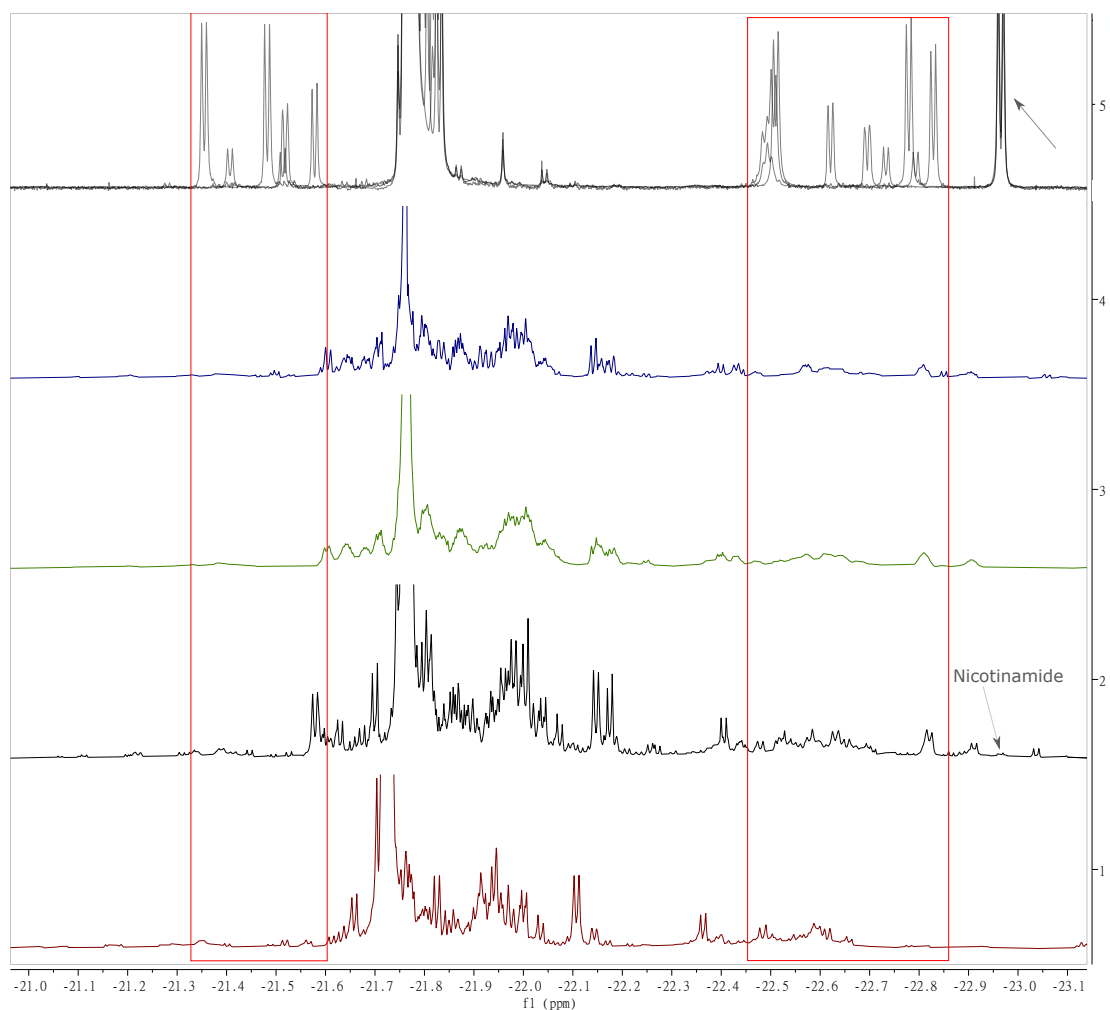


Figure 44. nh-PHIP spectra of 25 μM whole blood extract water-methanol layer. First sample (maroon) does not contain EDTA. In the second sample (black) EDTA (0.3 mM final concentration) was added straight to the NMR tube. For third spectrum (green) EDTA (0.3 mM final concentration) was mixed with the whole blood extract water-methanol layer prior to adding it to NMR tube. The fourth sample (blue) is the third sample to which another portion of EDTA was added (0.45 mM final concentration).

Figure 44 indicates that there are numerous hydride signals in the water-methanol layer of the whole blood extract. However, the amount of signals, their intensity and sharpness varies in terms of different sample preparation. Looking at the maroon and black spectra, without and with EDTA, respectively, it is clear that sample with EDTA has more signals. In essence, the addition of EDTA enhances the level of information that can be extracted from the spectra. For example, black spectrum shows clear presence of nicotinamide in the blood. Without EDTA, there is a small signal that is even smaller than its surrounding signals. However, with 2D ZQ-COSY, it can be attributed to nicotinamide.

Whole blood extract in prior mixing with EDTA causes broadening of the nh-PHIP signals. Addition of another portion of EDTA to the NMR tube sharpens some signals, but not to the extent seen in the black spectrum. Although, the approximate EDTA amount was calculated

from the average concentration of two-valence ions in blood, maybe even more is needed. The reason for this the difference in spectra between prior mixing and adding EDTA straight to the NMR tube is unclear. Maybe longer reaction time is needed for the ion exchange to take place. Therefore, additional experiments should be conducted to ascertain the reason for EDTA influence difference and to obtain maximum effectiveness.

5.2.2.5 Summary

ATP, ADP and AMP detection from blood is a challenging task. They are complexed with Mg^{2+} in human blood system. This complexation interferes with nh-PHIP measurements in such way that those phosphate signals are NMR invisible or shifted to a very different location in comparison to the bought analyte standard.

Chelex and EDTA were tested for the removal of Mg^{2+} from whole blood extract. EDTA removes some magnesium ions and ATP, ADP and AMP appear in the ^{31}P spectrum. However, with that pH was raised from 8.6 to 11.3, which affected the chemical shifts in 1H spectrum. Furthermore, the amount of Mg^{2+} removal is undetermined. Additionally, lyophilised whole blood extract cannot be dissolved only in methanol as neither ATP, ADP, nor AMP in blood are soluble in CD_3OD . Chelex nor EDTA treatment do not improve their solubility.

nh-PHIP spectrum of whole blood extract water-methanol layer contains numerous signals. The addition of EDTA increases the amount of information that can be obtained from the spectra, but no ATP, ADP and AMP were detected. Further experiments should be conducted to determine the specific reason for the differential influence of EDTA and to maximise its effectiveness.

5.3 Summary of experimental results

T_1 and T_2 relaxation are temperature and magnetic field dependent. In general increasing the temperature, decreases relaxation time constant of nh-PHIP catalyst complex on hydride signals of adenosine and nicotinamide. However, for some signals of adenosine complex, the longest relaxation time constant was observed in the room temperature measurement compared to the experiments conducted at 15°C and 35°C.

T_1 relaxation time constant of those hydrides increases with an increase in magnetic field strength. T_2 relaxation time constant, on the contrary, decreases for hydride signals of nicotinamide complex with an increase in magnetic field strength. However, for adenosine complex 400 MHz magnetic field showed longest relaxation time constants and 800 MHz fastest.

T_1 and T_2 relaxation time constants of adenosine and nicotinamide with 2H -labelled ligand and 2H -labelled co-substrate complex are prolonged compared to unlabelled ligand and

co-substrate. Difference is bigger for T_1 relaxation time constant. Additionally, ^2H -labelling of both iridium complex parts gives increase in spectral intensity. Intensity does not change much when only ligand or co-substrate are ^2H -labelled compared to $[\text{Ir}(\text{H})_2(\text{IMes})(\text{mtz})_2\text{X}]^+$ complex.

What is more, only ^2H -labelling of co-substrate makes the complex to be more temperature and analyte complexation site dependent. Only ^2H -labelling of ligand has bigger effect on relaxation time constants at 15°C .

nh-PHIP was applied to human whole blood extract, but due to blood's complex nature, ATP, ADP and AMP could not be detected. Complexation with Mg^{2+} interferes with nh-PHIP. Sample preparation methods to remove magnesium ions were applied. EDTA showed its potential on whole blood extract water-methanol layer. However, further experiments are needed to get more effect from EDTA and at the end measure blood plasma ATP, ADP and AMP levels.

Summary

The aim of this work was to determine whether the process of deuteration extends the relaxation time enough to yield additional enhancement of hyperpolarisation signals. Furthermore, to create method to detect biologically relevant analytes from blood in the lower magnetic field.

The first chapter gives an overview of the physical background of NMR spectroscopy and hyperpolarisation. The next chapter gives an insight into blood and its purpose as a diagnostic tool in healthcare. The third chapter takes a look at cancer cells. In particular, normal and malignant cells are compared and their energy metabolism is examined. The following chapter describes the development of the method. Conclusions are drawn there.

The development of the method was divided into two parts. The first part focuses on the relaxation time constants T_1 and T_2 . The experiments concluded that relaxation is influenced by many factors. These include the measurement temperature, the magnetic field strength, and the association-dissociation of the analyte with the iridium catalyst. In addition, deuteration of the catalyst ligand and co-substrate increases the hydride signals of the analytes. Furthermore, deuteration increases both the relaxation time constants T_1 and T_2 , but not significantly. Deuteration should be considered when analytes are present at concentrations near the detection limit.

The second part of the method development focused on whole blood extract and adenosine phosphates. More specifically, ATP, ADP and AMP from whole blood were investigated. This was challenging due to complexation with Mg^{2+} in the human blood system. Therefore, methods to remove magnesium complexation from phosphates were investigated. EDTA showed great potential, but further experiments are needed to annotate ATP, ADP and AMP from blood.

Most of the aims of the thesis were achieved. The effect of 2H -labelling in the nh-PHIP catalyst complex on the hydride signals of adenosine and nicotinamide as biologically relevant analytes was found. As well as the effect of 2H labelling on the nh-PHIP signals of the catalyst ligand and co-substrate. In addition, temperature and magnetic field effects on the relaxation time constants T_1 and T_2 were determined.

However, the optimised conditions of nh-PHIP were only applied to pure ATP, not to human blood. Further experiments are needed to find a way to remove the complexation of adenosine phosphates with magnesium. After that, ATP, ADP and AMP should be detectable from blood

with nh-PHIP. This could be followed by their detection from blood plasma.

Acknowledgements

The author of the thesis acknowledges the supervision and contributions of her supervisors Indrek Reile and Kerti Ausmees, who were comprehensively helpful in completing the thesis. Additionally, the author thanks Kaspar Klettenberg for his help with making conceptual figures. The author would like to express gratitude to Marina Kudrjašova from Tallinn University of Technology and Lauri Toom from University of Tartu for granting the author and supervisor access to their NMR spectrometers. ChatGTP and DeepL were used for language correction.

Bibliography

- [1] P. J. Hore. *Nuclear Magnetic Resonance. Second edition*. Oxford, United Kingdom: Oxford University Press, 2015.
- [2] A. Goldbourt. *Basics of NMR: Interactions, CW/FT, hardware, Bloch (lecture)*. Schloss Windischleuba, Germany: Oxford University Press Inc, 2023.
- [3] M. H. Levitt. *Spin Dynamics. Basics of Nuclear Magnetic Resonance. Second edition*. West Sussex, United Kingdom: John Wiley & Sons, Ltd, 2015.
- [4] T. Editors of Encyclopaedia Britannica. *Zeeman effect*. 13 September 2021. URL: <https://www.britannica.com/science/Zeeman-effect>. Read on 1 March 2023.
- [5] T. D. W. Claridge. *High-Resolution NMR Techniques in Organic Chemistry. Second Edition*. Oxford, Suurbritannia: Elsevier, 2009.
- [6] I. Reile. *Lühikursus TMR spektroskoopias*. 2013.
- [7] J. K. M. Sanders and B. K Hunter. *Modern NMR Spectroscopy. A Guide for Chemists. Second edition*. New York, USA: Oxford University Press Inc, 1993.
- [8] J. Keeler. *Understanding NMR Spectroscopy. Second Edition*. West Sussex, United Kingdom: John Wiley & Sons, Ltd, 2010.
- [9] R. Fraser et al. "Analysis of Complex Mixtures by Chemosensing NMR Using *para*-Hydrogen-Induced Hyperpolarization." In: *Accounts of Chemical Research* 55 (2022), 18321844. DOI: 10.1021/acs.accounts.1c00796.
- [10] *Parahydrogen*. 28 June 2013. URL: <https://www.york.ac.uk/chym/parahydrogen/>. Read on 2 March 2023.
- [11] P. Richardson et al. "Quantification of hyperpolarisation efficiency in SABRE and SABRE-Relay enhanced NMR spectroscopy." In: *Physical Chemistry Chemical Physics* 20 (2022), 18321844. DOI: 10.1039/C8CP05473H.
- [12] M. Hoffman. *Picture of Blood*. 23 June 2021. URL: <https://www.webmd.com/heart/anatomy-picture-of-blood>. Read on 25 October 2022.
- [13] *Blood Basics*. URL: <https://www.hematology.org/education/patients/blood-basics>. Read on 25 October 2022.
- [14] W. S. Mielczarek et al. "Microfluidic blood plasma separation for medical diagnostics: is it worth it?" In: *Lab Chip* 16 (18 2016), pp. 3441–3448. DOI: 10.1039/C6LC00833J.
- [15] L. Thomas. *Blood Plasma Components and Function*. 10 October 2018. URL: <https://www.news-medical.net/health/Blood-Plasma-Components-and-Function.aspx>. Read on 14 May 2023.

- [16] Lung National Heart and Blood Institute. *Blood Plasma Components and Function*. 22 March 2022. URL: <https://www.nhlbi.nih.gov/health/blood-tests>. Read on 14 May 2023.
- [17] G. B. Sonawane, K. V. Pansare, and S. K. Singh. *Recent Advances in Pharmaceutical Sciences. Chapter 1. Biology of Normal Cell and Cancer Cell*. Vol. 7. New Delhi: Akinik Publications, 2021.
- [18] A. I. Baba and C. Cătoi. *Comparative Oncology. Chapter 3. Tumor cell morphology*. Bucharest: The Publishing House of the Romanian Academy, 2007.
- [19] Biologydictionary.net Editors. *Adenosine Triphosphate (ATP)*. 20 January 2017. URL: <https://biologydictionary.net/atp/>. Read on 28 October 2022.
- [20] G. A. N. Gowda et al. "Simultaneous Analysis of Major Coenzymes of Cellular Redox Reactions and Energy Using ex Vivo ^1H NMR Spectroscopy". In: *Analytical Chemistry* 88.9 (2016), pp. 4817–4824. DOI: 10.1021/acs.analchem.6b00442.
- [21] E. Gout et al. "Interplay of Mg^{2+} , ADP, and ATP in the cytosol and mitochondria: Unravelling the role of Mg^{2+} in cell respiration". In: *The Proceedings of the National Academy of Sciences* 111.43 (2014), E4560–E4567. DOI: 10.1073/pnas.1406251111.
- [22] A. Klepinin et al. "Stable Isotope Tracing Uncovers Reduced $^-$ -ATP Turnover and Metabolic Flux Through Mitochondrial-Linked Phosphotransfer Circuits in Aggressive Breast Cancer Cells". In: *Frontiers in Oncology* 12 (2022). DOI: 10.3389/fonc.2022.892195.
- [23] D. Jia et al. "Elucidating the Metabolic Plasticity of Cancer: Mitochondrial Reprogramming and Hybrid Metabolic States." In: *Cells* 7.3 (2018). DOI: 10.3390/cells7030021.
- [24] O. A. Deshpande and S.S. Mohiuddin. "Biochemistry, Oxidative Phosphorylation." In: *StatPearls [Internet]* (2022). URL: <https://www.ncbi.nlm.nih.gov/books/NBK553192/>.
- [25] E. Rapaport and J. Fontaine. "Generation of extracellular ATP in blood and its mediated inhibition of host weight loss in tumor-bearing mice". In: *Biochemical Pharmacology* 38.23 (1989), pp. 4261–4266. DOI: 10.1016/0006-2952(89)90524-8.
- [26] R. Savka and H. Plenio. "Facile Synthesis of [(NHC)MX(Cod)] and [(NHC)MCl(CO) $_2$] (M = Rh, Ir; X = Cl, I) Complexes." In: *Dalton Transactions* 44.3 (2014), pp. 891–893. DOI: 10.1039/C4DT03449J.
- [27] M. J. Cowley et al. "Iridium N-Heterocyclic Carbene Complexes as Efficient Catalysts for Magnetization Transfer from Para-Hydrogen." In: *Journal of the American Chemical Society* 133.3 (2011), pp. 6134–6137. DOI: 10.1021/ja200299u.
- [28] M. A. Seefeld; M. B. Rouse; D. A. Heerding; S. Peace; D. S. Yamashita; K. C. McNulty. "Inhibitors of AKT Activity". WO2008/098104 A1 (United States). 2008.
- [29] G. A. N. Gowda and D. Raftery. "Whole Blood Metabolomics by ^1H NMR Spectroscopy Provides a New Opportunity To Evaluate Coenzymes and Antioxidants". In: *Analytical Chemistry* 89 (2017), pp. 4620–4627. DOI: 10.1021/acs.analchem.7b00171.

- [30] N. J. Wood et al. "Detection of Picomole Amounts of Biological Substrates by para-Hydrogen-Enhanced NMR Methods in Conjunction with a Suitable Receptor Complex". In: *Journal of the American Chemical Society* 129.36 (2007), pp. 11012–11013. DOI: 10.1021/ja074286k.
- [31] *Enantiomers vs. Diastereomers*. 9 March 2023. URL: <https://chemistrytalk.org/enantiomers-diastereomers/>. Read on 16 March 2023.
- [32] P. J. Rayner et al. "Delivering strong ¹H nuclear hyperpolarization levels and long magnetic lifetimes through signal amplification by reversible exchange". In: *PNAS* 114 (2017), pp. 3188–3194. DOI: 10.1073/pnas.1620457114.
- [33] N. G. Holm. "The significance of Mg in prebiotic geochemistry." In: *Geobiology* 10 (2012), pp. 269–279. DOI: 10.1111/j.1472-4669.2012.00323.x.
- [34] J.-C. Liao et al. "The conformational states of Mg-ATP in water". In: *European biophysics journal* 33 (2004), pp. 29–37. DOI: 10.1007/s00249-003-0339-2.
- [35] M. W. Gorman, E. O. Feigl, and C. W. Buffington. "Human plasma ATP concentration". In: *Clinical Chemistry* 53.2 (2007), pp. 318–325. DOI: 10.1373/clinchem.2006.076364.
- [36] *Chelex 100 Chelating Resin*. URL: <https://www.bio-rad.com/en-ee/product/chelex-100-chelating-resin?ID=08197b5d-95fa-4285-be0e-a140bd734f95>. Read on 14 April 2023.
- [37] *Chelex 100*. URL: <https://www.biosynth.com/p/FC180017/11139-85-8-chelex-100>. Read on 14 April 2023.
- [38] Z. Mohammadi, S. Shalavi, and H. Jafarzadeh. "Ethylenediaminetetraacetic acid in endodontics". In: *European Journal of Dentistry* 7 (2013), S135–S142. DOI: 10.4103/1305-7456.119091.
- [39] M. Bozic. *Purple top tubes: your impact on research*. 14 January 2021. URL: <https://stanfordbloodcenter.org/purple-top-tubes-your-impact-on-research/>. Read on 14 April 2023.

Appendices

Appendix 1 - Tables with T_1 and T_2 relaxation time constants

Table 5. Temperature-deuteration experiment T1 relaxation time constants.

Temperature	Region	T1 relaxation time constant (ms)			
		IMes + mtz	IMes-d ₂₂ + mtz	IMes + mtz-d ₅	IMes-d ₂₂ + mtz-d ₅
15°C	A1	816	816	950	772
	A2	803	1136	702	931
	A3	848	1207	784	981
	A4	833	1124	674	1109
	B	940	1126	1084	1315
25°C	A1	624	738	806	943
	A2	680	714	779	969
	A3	966	1024	923	1383
	A4	936	1169	1262	1682
	B	814	933	940	1276
35°C	A1	344	413	394	410
	A2	399	442	422	456
	A3	802	976	874	1055
	A4	812	983	896	1099
	B	500	553	528	563

Table 6. Temperature-deuteration experiment T2 relaxation time constants.

		T2 relaxation time constant (ms)			
Temperature	Region	IMes + mtz	IMes-d ₂₂ + mtz	IMes + mtz-d ₅	IMes-d ₂₂ + mtz-d ₅
15°C	A1	227	280	243	296
	A2	260	225	177	236
	A3	435	512	516	536
	A4	666	772	568	619
	B	511	642	586	650
25°C	A1	194	221	183	227
	A2	189	211	199	233
	A3	471	516	384	616
	A4	462	517	509	729
	B	381	418	405	503
35°C	A1	149	149	143	158
	A2	162	155	161	167
	A3	388	431	442	451
	A4	417	475	478	503
	B	212	213	221	231

Table 7. T_1 and T_2 relaxation time constants for 800 and 400 MHz spectrometer measurements of deuterated and non-deuterated complexes and their ratios.

Field strength	Signal region	Non-deuterated	Deuterated	Ratio of deuterated and non-deuterated values
		T_1 relaxation (ms)		
800 MHz	A1	610	943	1.55
	A23	820	1165	1.42
	A4	931	1649	1.77
	B	814	1277	1.57
		T_2 relaxation (ms)		
	A1	187	251	1.35
	A23	281	388	1.38
	A4	398	646	1.62
	B	377	498	1.32
	400 MHz		T_1 relaxation (ms)	
A1		518	645	1.24
A23		483	773	1.60
A4		532	759	1.43
B		671	907	1.35
		T_2 relaxation (ms)		
A1		381	404	1.06
A23		414	489	1.18
A4		528	614	1.16
B		428	495	1.16

Table 8. T_1 and T_2 relaxation time constants for 800, 400 and 200 MHz spectrometer measurements of deuterated and non-deuterated complexes and their ratios.

Field strength	Signal region	Non-deuterated	Deuterated	Ratio of deuterated and non-deuterated values
		T_1 relaxation (ms)		
800 MHz	A	789	1150	1.46
		812	1264	1.56
	T_2 relaxation (ms)			
	B	280	324	1.16
374		478	1.28	
400 MHz	T_1 relaxation (ms)			
	A	503	734	1.46
		669	902	1.35
	T_2 relaxation (ms)			
B	425	486	1.14	
	424	496	1.17	
200 MHz	T_1 relaxation (ms)			
	A	438	689	1.57
		638	912	1.43
	T_2 relaxation (ms)			
B	358	430	1.20	
	438	514	1.17	